Master's Degree Final Project
Máster Universitario en Ingeniería Aeronáutica

Probabilistic Aircraft Conflict Detection Using Transformation of Random Variables

Detección Probabilística de Conflictos entre Aeronaves utilizando Transformación de Variables Aleatorias

Autor: Eulalia Hernández Romero

Tutor: Alfonso Valenzuela Romero

Dep. Ingeniería Aeroespacial y Mecánica de Fluidos
Escuela Técnica Superior de Ingeniería
Universidad de Sevilla

Sevilla, 2016

Master's Degree Final Project
Máster Universitario en Ingeniería Aeronáutica

Probabilistic Aircraft Conflict Detection Using Transformation of Random Variables

Detección Probabilística de Conflictos entre Aeronaves utilizando Transformación de Variables Aleatorias

Author:
Eulalia Hernández Romero

Tutor:
Alfonso Valenzuela Romero
Profesor Contratado Doctor Interino

Dep. Ingeniería Aeroespacial y Mecánica de Fluidos
Escuela Técnica Superior de Ingeniería
Universidad de Sevilla

Sevilla, 2016

Resumen

En este proyecto se estudia la situación de conflicto en la que dos aeronaves se aproximan con velocidad, rumbo y altitud constante en el mismo nivel de vuelo, bajo la presencia de vientos desconocidos definidos por su función de densidad de probabididad.

Se considera que un conflicto se produce cuando se predice que en el futuro las aeronaves se encontrarán en pérdida de separación, es decir, cuando se predice que las aeronaves se encontrarán a una distancia entre ellas menor que un margen mínimo de separación. El conflicto se caracteriza por una serie de *indicadores*, tales como la mínima distancia entre aeronaves, el instante de tiempo en el que se alcanza esta distancia o la probabilidad de que este se produzca.

En este proyecto se realiza un estudio probabilístico usando *transformación de variables aleatorias*. Con este método, es posible obtener la función de densidad de los indicadores a partir de una transformación de la función de densidad del viento. Los resultados obtenidos son comparados y validados usando el *método de Monte Carlo*.

Para dos escenarios diferentes, se estudian los efectos de las propiedades estadísticas del viento, tales como su media o varianza, y de la velocidad de las aeronaves sobre los indicadores.

Abstract

The aim of this project is to analyse the conflict between two approaching aircraft flying at a constant airspeed, course and altitude for uncertain winds, which are defined by their *probability density functions* (PDFs).

The conflict is characterized by a series of *indicators*, such as the minimum distance between aircraft, the time to minimum distance or the probability of conflict. A loss of separation is considered to exist if the minimum distance is found to be smaller than a minimum separation margin.

A probabilistic analysis is performed using *transformation of random variables*. In this method, the indicator's PDFs are computed by a transformation of the wind speed PDFs. The results are validated using the *Monte Carlo method*. The effects of the statistical parameters of the wind and the aircraft airspeeds are analysed for two different scenarios.

Contents

1 Introduction

1.1 Motivation

The Air Traffic Management (ATM) system is a large and complex system which contains a vast number of agents, such as aircraft, pilots, controllers and airports, that interact with each other in a complex network. Inside the ATM, the Air Traffic Control (ATC) is responsible for organizing the flow of air traffic, provide information for pilots and preventing hazardous operations. The complexity of the interactions of ATM members, that are non-linear in most situations and can lead to emergent behaviours, combined with the increasing levels of air traffic, makes necessary the development of tools to assist ATC operations.

The European airspace is among the busiest in the world. As a response to the increasing capacity problems, the European Commission created in 1999 the Single European Sky (SES) initiative, with the objective of drawing a common airspace and air navigation services for all European countries. In 2005, the political vision and high level goals for the SES were stated, which include increasing the capacity and safety of the ATM system and reducing the costs and environmental impact of European flights. The Single European Sky ATM Research (SESAR) is the technological pillar of SES, devoted to develop the state-of-the-art technological systems and components required to meet SES goals. Among SESAR's lines of investigation, an approach that can improve current prediction and optimisation mechanisms is to model, analyse, and manage the uncertainty present in ATM.

Several sources of uncertainty are present in ATM. The ComplexWorld Research Network [8] identifies the following types:

- **Data uncertainty.** This source of uncertainty comes from an incomplete knowledge of the aircraft data or incorrect models. Some typical examples are uncertain GPS position, aircraft take-off weight or oversimplified aircraft models.
- **Operational uncertainty** Human decisions are a clear source of uncertainty: they are extremely difficult to predict and can have a very significant influence on ATM operations. Imprecision in the execution of ATC instructions by pilots is an example of this type of uncertainty.
- **Equipment uncertainty** This type refers to problems in equipment, from aircraft breakdown to total system failure.
- **Weather uncertainty** The atmosphere is a complex system whose exact behaviour is practically impossible to predict. Weather can only be predicted in a satisfying way in a relatively short horizon, which causes flight plans based on early meteorological estimations to be far away from the real scenario.

Among these sources, weather uncertainty has the greatest impact on ATM operations. The limited knowledge about future meteorology conditions, such as wind velocity, fog, snowfall or storms, is responsible for much of the delays and flight cancellations, which negatively affects ATM efficiency and translates to extra costs for airlines and air navigation service providers.

The analysis of the impact of weather uncertainties in conflict detection may benefit ATM performance by improving its safety and efficiently levels. Some applications would include the development of ATC support tools for conflict detection and resolution tasks or optimal conflict-resolution algorithms.

1.2 Trajectory prediction based on ensemble weather forecasts

While deterministic meteorological forecasts have long been used in trajectory prediction and, as for today, are still the standard in ATM applications, a lot of efforts have been made to introduce uncertainty information in trajectory prediction systems . One of today's trends is using *Ensemble Prediction Systems*, which are based on repeatedly running a deterministic model with a different starting state , and/or different physical parametrizations, to obtain an ensemble of forecasts [3] [12] (see Fig. 1.1). These ensemble of forecasts aim to generate a representative sample of the possible future states of the atmosphere.

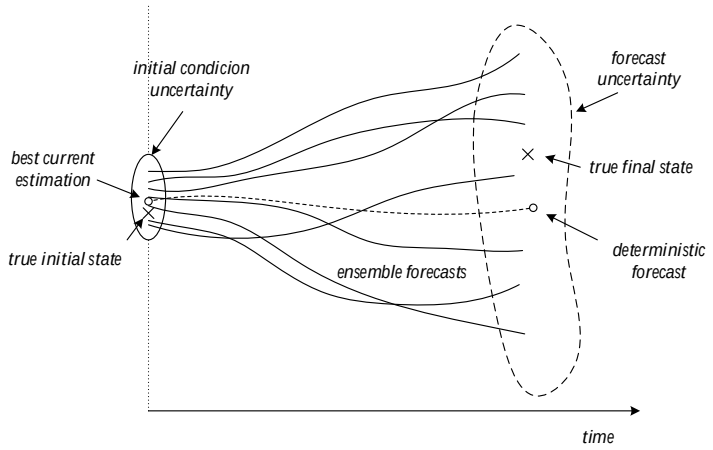

Figure 1.1 Schematic of deterministic forecast vs ensemble forecast.

An ensemble forecast is a collection of typically 10 to 50 weather forecasts or members. Some of these EWF are reviewed in [3]: Prévision d'Ensemble Action de Recherche Petite Echelle Grande Echelle (PEARP), a French model with 35 members; Met Office Global and Regional Ensemble Prediction System (MOGREPS); from UK Met Office consisting of 12 members; and the EPS of the European ECMWF, with 51 members. These ensembles can be combined to produce a SUPER multi-model ensemble, consisting of 98 members.

SESAR's IMET project (*Investigation of the optimal approach for future trajectory prediction systems to use METeteorological uncertainty information*) aimed to quantify the sensibility of trajectory parameters to uncertainty in meteorological forecast. In IMET project [1], two approaches for probabilistic trajectory prediction based on ensemble weather forecast (EWF) are described (see Figure 1.2):

b) **Probabilistic trajectory prediction**. In this approach, the probability distribution of the trajectory parameters of interest are directly derived from a probabilistic distribution of the weather quality of interest using a *probabilistic trajectory predictor* (PTP). A previous statistical post-processing of the forecast ensemble is necessary to create the weather probability density function.

b) **Ensemble trajectory prediction**. This second approach is based on repeatedly applying a *deterministic trajectory predictor* (DTP) for each member of the ensemble weather forecast, which leads to an ensemble of trajectories that can be post-processed to obtain its statistical properties.

While the IMET project followed the second approach, the work presented in this project follows the first one.

1.3 Objectives

This project is devoted to analyse the conflict between two approaching aircraft flying at constant airspeed, course and altitude. The aircraft fly on the cruise phase in the same airspace, where the weather conditions, in particular the wind, are uncertain.

A conflict occurs when a loss of separation is predicted to exist in the future, that is to say, the distance between aircraft is predicted to be smaller than a minimum separation margin at some point of their trajectory. The conflict is characterized by a series of *indicators*, that will describe the severity of the situation. Parameters

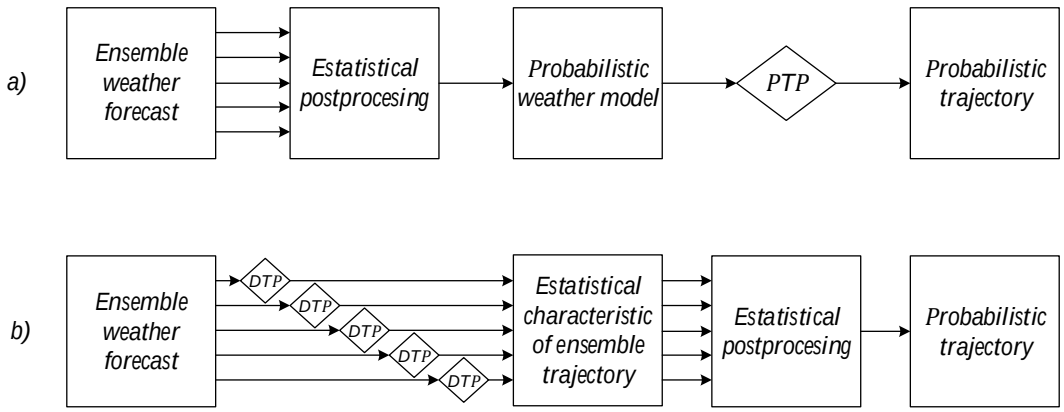

Figure 1.2 Probabilistic trajectory prediction based on ensemble weather forecast.

such as the minimum distance between aircraft, the time to minimum distance or the duration of the loss of separation are obtained. One of the most relevant indicators studied in this project is the *probability of a conflict* for a given scenario.

A probabilistic analysis is performed using a numerical approximation to the *transformation of random variables* method. With this method, the indicator's *probability density functions* (PDFs) are computed by evolving the wind speed PDFs. The numerical results are validated using the *Monte Carlo method*. The effects of the wind statistical parameters and the aircraft airspeeds are analysed for two different scenarios.

1.4 Outline

The present document is structured as follows. In Chapter 2, a description of the problem under consideration is presented: the general scenario is described and the conflict between the aircraft is defined by a series of indicators. The governing equations for the problem are formulated. Next, in Chapter 3, the application of the transformation of random variables and Monte Carlo methods to the present problem is addressed. The basics of the two methods will be described, as well as their numerical application. The final results are presented in Chapter 4, where the PDFs for the sought indicators are depicted. The influence of wind statistical parameters (such as its mean and standard deviation) and the aircraft airspeed on the conflict are also analysed. Finally, in Chapter 5, some conclusions and future work are presented.

2 Problem Formulation

A description of the problem scenario is presented in this chapter. The equations that describe the behaviour of the aircraft and their interaction are presented and analysed.

The indicators herein chosen to describe the conflict between the aircraft are also introduced. Additionally, the probabilistic wind model used in this project is defined.

2.1 General scenario

The scenario under analysis in this project is depicted in Figure 2.1. The case of two aircraft, A and B, that fly on the cruise phase with approaching trajectories is considered. Being the wind uncertain, the aircraft may or may not end up by losing a desired separation necessary for a conflict to be detected.

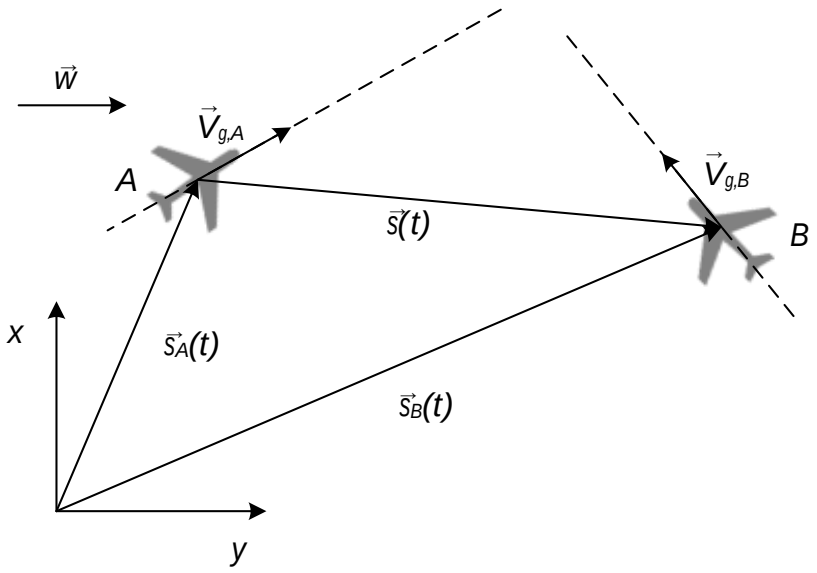

Figure 2.1 General conflict scenario.

The conflict scenario under consideration is described by the following assumptions:

- the two aircraft fly in the same airspace and flight level;
- the course (ψ_A and ψ_B) and airspeed (V_A and V_B) of both aircraft are constant and, alongside their initial positions ($\vec{s}_{0A}$ and $\vec{s}_{0B}$), they are perfectly known;
- the aircraft are considered to be close enough so as to be affected by the same wind;

- the wind $\vec{w}$ is uncertain; and
- initially, the distance between aircraft is greater than a desired separation margin D, that is to say, there is no loss of separation at $t = 0$.

In order to describe the position of the aircraft $\vec{s}_A(t)$ and $\vec{s}_B(t)$, an earth-fixed reference system is used, where the x-axis is pointing towards the North and the y-axis is pointing East. The aircraft position is then described by

$$\begin{aligned} \vec{s}_A(t) &= \vec{s}_{A0} + \vec{V}_{gA}t \\ \vec{s}_B(t) &= \vec{s}_{B0} + \vec{V}_{gB}t \end{aligned} \tag{2.1}$$

where V_{gA} and V_{gB} are the aircraft ground speeds, which in turn are given by

$$\begin{aligned} \vec{V}_{gA}(t) &= \vec{V}_A(t) + \vec{w} \\ \vec{V}_{gB}(t) &= \vec{V}_B(t) + \vec{w} \end{aligned} \tag{2.2}$$

Notice that inasmuch as the wind is uncertain and the course and airspeeds of the aircraft are fixed, the magnitudes of $\vec{V}_{gA}$ and $\vec{V}_{gB}$ are also uncertain and so are the directions of $\vec{V}_A$ and $\vec{V}_B$.

The relative motion between the aircraft is also a matter of importance in order to describe the conflict situation. The relative position between the two aircraft $\vec{s}(t) = \vec{s}_B(t) - \vec{s}_A(t)$ can be computed as

$$\vec{s}(t) = \vec{s}_{B0} - \vec{s}_{A0} + (\vec{V}_{gB} - \vec{V}_{gA})t = \vec{s}_0 + \vec{V}_g t \tag{2.3}$$

where $\vec{s}_0$ and $\vec{V}_g$ are the relative initial position and relative ground speed vectors, respectively. The distance between the aircraft at a given time $d(t)$ can now be computed as the magnitude of the relative position, so one can write

$$d(t) = ||\vec{s}(t)|| = \sqrt{(\vec{s}_0 + \vec{V}_g t).(\vec{s}_0 + \vec{V}_g t)} = \sqrt{s_0^2 + 2\vec{s}_0\vec{V}_g t + V_g^2 t^2} \tag{2.4}$$

being s_0 and V_g the magnitudes of the relative initial position and relative ground speed vectors.

2.2 Conflict indicators

In this section, the indicators chosen to characterize the conflict are presented. These parameters are defined as follows.

- **Time to minimum distance** $t_{d_{min}}$

  The instant of time when the distance between the aircraft reaches a minimum can be obtained by setting to zero the derivative of the function $d(t)$ given by (2.4) with respect to the time t, so one has

  $$\frac{d(d(t))}{dt} = \frac{1}{2}\frac{2\vec{s}_0.\vec{V}_g + 2V_g^2 t}{d(t)} = 0 \rightarrow t_{d_{min}} = \frac{-\vec{s}_0.\vec{V}_g}{V_g^2} \tag{2.5}$$

  Given that the aircraft have approaching courses, the existence of a minimum in the function $d(t)$ is always guaranteed at $t_{d_{min}} > 0$.

- **Minimum distance** d_{min}

  The value of the minimum distance between the two aircraft can be computed by evaluating the equation (2.4) in the instant of time $t_{d_{min}}$:

  $$d_{min} = \sqrt{s_0^2 - 2\vec{s}_0\vec{V}_g\frac{\vec{s}_0.\vec{V}_g}{V_g^2} + V_g^2\frac{(\vec{s}_0.\vec{V}_g)^2}{V_g^4}} = \sqrt{s_0^2 - \frac{(\vec{s}_0.\vec{V}_g)^2}{V_g^2}} \tag{2.6}$$

  This parameter can be seen as an indicator of the conflict intensity.

- **Probability of loss of separation at time** t $P[d(t) \leq D]$

  In the general scenario considered in this project, the two aircraft fly at the same altitude, so a loss of separation will exist if the horizontal distance between them ($d(t)$) is smaller than a desired separation margin D, typically 5NM.

  $$d(t) \leq D \tag{2.7}$$

  The probability of the occurrence of a loss of separation at a given time can be expressed as the probability of the function $d(t)$ of being less or equal than D, or $P[d(t) \leq D]$.

  Additionally, an interesting point of view would be to obtain the probability of loss of separation for aircraft i given a distance r_i along its trajectory, that could be expressed as

  $$P\left[d\left(\frac{r_i}{V_{gi}}\right) \leq D\right] \tag{2.8}$$

- **Probability of conflict** P_{con}

  The probability of conflict for the whole trajectory is given by the probability of the indicator d_{min} of being smaller than the separation margin. This can be expressed as

  $$P[d_{min} \leq D] \tag{2.9}$$

  and does not depend on the time.

- **Duration of the loss of separation** Δt

  In the case of a violation of the separation minima, the duration of the loss of separation is also a parameter of interest. One can obtain this indicator by setting equation (2.4) equal to D:

  $$d(t) = D \rightarrow s_0^2 + 2t\vec{s_0}\cdot\vec{V}_g + V_g^2 t^2 = D^2 \tag{2.10}$$

  which is a second-degree equation whose solutions are

  $$t = \frac{-\vec{s}_0.\vec{V}_g}{V_g^2} \pm \sqrt{\frac{(\vec{s}_0.\vec{V}_g)^2}{V_g^4} - \frac{(s_0^2 - D^2)}{V_g^2}} \tag{2.11}$$

  The smaller solution will correspond to the instant of time when the loss of separation is predicted to start whereas the bigger one will correspond to the instant of time when the loss of separation is predicted to end. The duration of the loss of separation can be computed from the previous equation as the difference between these two solutions

  $$\Delta t = 2\sqrt{\frac{(\vec{s}_0.\vec{V}_g)^2}{V_g^4} - \frac{(s_0^2 - D^2)}{V_g^2}} \tag{2.12}$$

  In terms of t_{dmin}, this indicator can be expressed as

  $$\Delta t = 2\sqrt{t_{dmin}^2 - \frac{(s_0^2 - D^2)}{V_g^2}} \tag{2.13}$$

  Notice that this parameter is only defined when the radicand has a positive value, that is, when a conflict exists

2.3 Velocity uncertainty

The indicators presented in the previous section are mostly dependent on three factors: s_0^2, $\vec{s}_0.\vec{V}_g$ and V_g^2. Being the initial positions of the aircraft perfectly known, the vector $\vec{s}_0$ is certain, and so it is its modulus s_0^2. In consequence, the source of uncertainty must devolve upon $\vec{s}_0.\vec{V}_g$ and V_g^2.

Taken this into account, it is now necessary to obtain the expression of $\vec{V}_g$ in terms of the wind. Given that the relative ground velocity expressed as

$$\vec{V}_g = \vec{V}_{gB} - \vec{V}_{gA} = \vec{V}_B + \vec{w} - (\vec{V}_A + \vec{w}) = \vec{V}_B - \vec{V}_A \tag{2.14}$$

does not depend directly on the wind, the expressions of the airspeeds $\vec{V}_A(\vec{w})$ and $\vec{V}_B(\vec{w})$ are to be sought. These equations can be computed from the wind triangles (see Figure 2.2) as follows.

$$\vec{V}_A = V_A \begin{bmatrix} cos(\chi_A) \\ sin(\chi_A) \end{bmatrix} = V_A \begin{bmatrix} cos\left(\psi_A - arcsin\left(\frac{w_{c,A}}{V_A}\right)\right) \\ sin\left(\psi_A - arcsin\left(\frac{w_{c,A}}{V_A}\right)\right) \end{bmatrix} \tag{2.15}$$

$$\vec{V}_B = V_B \begin{bmatrix} cos(\chi_B) \\ sin(\chi_B) \end{bmatrix} = V_B \begin{bmatrix} cos\left(\psi_B - arcsin\left(\frac{w_{c,B}}{V_B}\right)\right) \\ sin\left(\psi_B - arcsin\left(\frac{w_{c,B}}{V_B}\right)\right) \end{bmatrix} \tag{2.16}$$

where χ_i is the heading of the aircraft i, ψ_i the course and $w_{c,i}$ the *crosswind* affecting that aircraft. The magnitude V_i of these vectors is known. The crosswinds can be expressed in terms of the North and East components of the wind as

$$w_{c,A} = w_y cos\psi_A - w_x sin\psi_A \tag{2.17}$$

$$w_{c,B} = w_y cos\psi_B - w_x sin\psi_B \tag{2.18}$$

These terms are considered to be positive when the crosswind comes from the left wind.

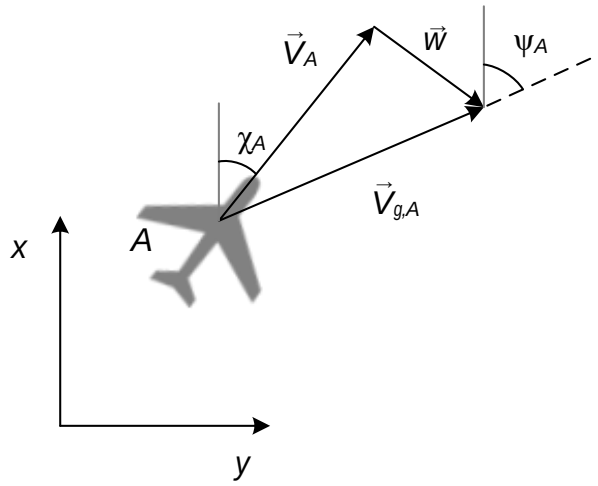

Figure 2.2 Wind triangle for aircraft A.

Finally, from equation (2.14), the relative ground speed is given by

$$\vec{V}_g = V_B \begin{bmatrix} cos\left(\psi_B - arcsin\left(\frac{w_{c,B}}{V_B}\right)\right) \\ sin\left(\psi_B - arcsin\left(\frac{w_{c,B}}{V_B}\right)\right) \end{bmatrix} - V_A \begin{bmatrix} cos\left(\psi_A - arcsin\left(\frac{w_{c,A}}{V_A}\right)\right) \\ sin\left(\psi_A - arcsin\left(\frac{w_{c,A}}{V_A}\right)\right) \end{bmatrix} \tag{2.19}$$

Notice that the only terms in the previous equation that introduce uncertainty are the crosswinds affecting the aircraft, $w_{c,A}$ and $w_{c,B}$. The crosswinds are modulated in this expression by each aircraft velocity, V_A and V_B. This means that the bigger the aircraft airspeeds are, the less the conflict situation is affected by the wind uncertainty.

On the other hand, in the ground speeds expressions for each aircraft $V_{g,A}$ and $V_{g,B}$, the uncertainty is brought in by the crosswinds and also by the along-track winds (see equation 2.2).

2.4 Probabilistic wind model

In this project, the wind velocity is given by its *zonal component* w_y, in the west-east direction, and its *meridional component* w_x, in the north-south direction. These components are uncertain and are considered to be independent.

The method presented in this work is applicable to any statistical distribution, so any model of uncertain wind could be used, such as a normal or gamma distribution. Given the opportunity, a wind PDF calibrated by means of processed forecast ensembles could be used. The approach to obtain the PDF of the wind components using weather ensemble forecasting can be summarize as follows:

Suppose that the ensemble has n members. The first step would involve obtaining for each wind component and location the sample values $\{w_{x,1},\dots,w_{x,n}\}$ and $\{w_{y,1},\dots w_{y,n}\}$. Next, one must assume that each wind component follows a particular distribution. Finding a suitable distribution for this purpose is one of the open challenges in this problem. Finally, the parameters of the chosen distribution are estimated from the sample.

For the sake of simplicity, the wind components are considered to be distributed as *uniform continuous* random variables in this project.

The probability density function of the wind component w_i is given by equation (2.20), with an average value of $E[w_i] = \bar{w}_i$ and a half-width δ_{w_i}. In Figure 2.3, the wind component w_i PDF is depicted.

$$f_{w_i}(w_i) = \begin{cases} \frac{1}{2\delta_{w_i}}, & w_i \in [\bar{w}_i - \delta_{w_i}, \bar{w}_i + \delta_{w_i}] \\ 0 & \text{otherwise} \end{cases} \tag{2.20}$$

The variance of w_i is given by

$$Var[w_i] = E[w_i^2] - (E[w_i])^2 = \frac{1}{3}\delta_{w_i}^2 \tag{2.21}$$

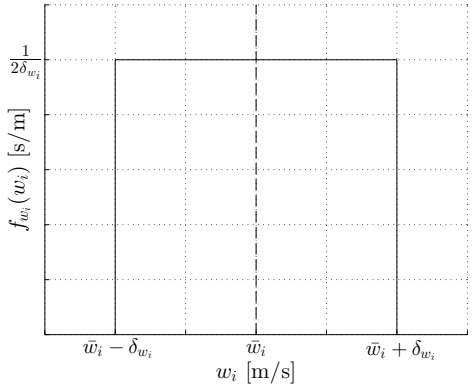

Figure 2.3 Wind component w_i uniform distribution.

Considering that the two wind components w_x and w_y are statistically independent, the *joint density function* $f_{w_x,w_y}(w_x,w_y)$ can be expressed as follows

$$f_{w_x,w_y}(w_x,w_y) = f_{w_x}(w_x)\cdot f_{w_y}(w_y) = \frac{1}{4}\frac{1}{\delta w_x \delta w_y}, \qquad w_i \in [\bar{w}_i - \delta w_i, \bar{w}_i + \delta w_i] \tag{2.22}$$

3 Obtaining probability density functions for two random variables

In this chapter, the computation of the *probability density function* (PDF) of the indicators described in Section 2.2, given a wind speed probability distribution, is presented. Some important statistics, such as the *mean* and the *standard deviation*, are also obtained.

Firstly, in Section 3.1, the transformation of two random variables applied to obtain the sought PDF is explained. The equations that are being particularized and used in this analysis and the implemented numerical procedure are presented.

Secondly, the application of the Monte Carlo method to the problem is addressed in Section 3.2.

3.1 Transformation of two random variables

Let us consider two random variables u_1 and u_2 with a known joint probability function $f_{u_1,u_2}(u_1,u_2)$ whose domain is the set $R \in \mathbb{R}^2$. Let v_1 and v_2 be two random variables

$$\begin{aligned} v_1 &= g_1(u_1,u_2) \\ v_2 &= g_2(u_1,u_2) \end{aligned} \tag{3.1}$$

whose density function $f_{v_1,v_2}(v_1,v_2)$ is to be obtained. Assuming that $g_1(u_1,u_2)$ and $g_2(u_1,u_2)$ is a *bijective transformation* that maps the set R of the u_1u_2 plane onto the set S of the v_1v_2 plane, one could express random variables as $u_1 = h_1(v_1,v_2)$ and $u_2 = h_2(v_1,v_2)$. The sought joint probability density function is then given by

$$f_{v_1,v_2}(v_1,v_2) = f_{u_1,u_2}(h_1(v_1,v_2),h_2(v_1,v_2)) \cdot |J(v_1,v_2)| \tag{3.2}$$

where J is the *Jacobian* of the transformation, which can be computed as

$$J = \begin{vmatrix} \frac{\partial u_1}{\partial v_1} & \frac{\partial u_1}{\partial v_2} \\ \frac{\partial u_2}{\partial v_1} & \frac{\partial u_2}{\partial v_2} \end{vmatrix} = \begin{vmatrix} \frac{\partial h_1(v_1,v_2)}{\partial v_1} & \frac{\partial h_1(v_1,v_2)}{\partial v_2} \\ \frac{\partial h_2(v_1,v_2)}{\partial v_1} & \frac{\partial h_2(v_1,v_2)}{\partial v_2} \end{vmatrix} \tag{3.3}$$

In the problem addressed in this project, the random variable v_1 would be one of the parameters described in the previous chapter: $d(t)$, d_{min}, $t_{d_{min}}$ and Δt. Being the north and east components of the wind the source of uncertainty, w_x and w_y take the place of u_1 and u_2.

One might notice that the random variable of interest is now a one-dimensional function of w_x and w_y. In order to compute the density function $f_{v_1}(v_1)$ in this case, let us use v_2 as an *auxiliary variable* . The joint density $f_{v_1,v_2}(v_1,v_2)$ is computed from (3.2), function that can be integrated over v_2 to obtain the marginal density function

$$f_{v_1}(v_1) = \int_{-\infty}^{\infty} f_{v_1,v_2}(v_1,v_2)dv_2 \tag{3.4}$$

In this work, the random variable w_y has been chosen to be the auxiliary variable, so as to simplify the Jacobian expression, which is now determined as

$$J = \begin{vmatrix} \frac{\partial w_x}{\partial v_1} & \frac{\partial w_x}{\partial w_y} \\ \frac{\partial w_y}{\partial v_1} & \frac{\partial w_y}{\partial w_y} \end{vmatrix} = \begin{vmatrix} \frac{\partial w_x}{\partial v_1} & \frac{\partial w_x}{\partial w_y} \\ 0 & 1 \end{vmatrix} = \left| \frac{\partial w_x(v_1, w_y)}{\partial y} \right| \tag{3.5}$$

Next, the equation (3.4) is particularized for the uniform distribution considered in this work as

$$f_{v_1}(v_1) = \int_{w_y} f_{v_1,w_y}(v_1, w_y) dw_y = \frac{1}{4} \frac{1}{\delta w_x \delta w_y} \int_{w_y} \left| \frac{\partial w_x(v_1, w_y)}{\partial v_1} \right| dw_y \tag{3.6}$$

where the limits of integration are determined by the transformed set S in the $v_1 w_y$ plane.

Once the PDF $f_{v_1}(v_1)$ is known, the mean and the typical deviation of v_1 can be computed as follows

$$E[v_1] = \int_{-\infty}^{\infty} v_1 f_{v_1}(v_1) dv_1 \tag{3.7}$$

$$\sigma[v_1] = \sqrt{\int_{-\infty}^{\infty} (v_1 - E[v_1])^2 f_{v_1}(v_1) dv_1} \tag{3.8}$$

3.1.1 Non-monotonic functions

The previous procedure is only to be applied when $v_1 = g_1(w_x, w_y)$ is an invertible function in the domain of f_{w_x,w_y} and the partial derivative $\partial w_x / \partial v_1$ exists and is continuous. However, this might not be the case of some indicators in determined scenarios.

For instance, let us consider the variable d_{min}, which for a given scenario adopts the non-monotonic behaviour depicted in Figure 3.1. Furthermore, one can observe that the partial derivative is not even defined in some points of the domain. In this particular scenario, the two aircraft collide ($d_{min} = 0$) for certain values of the wind speed.

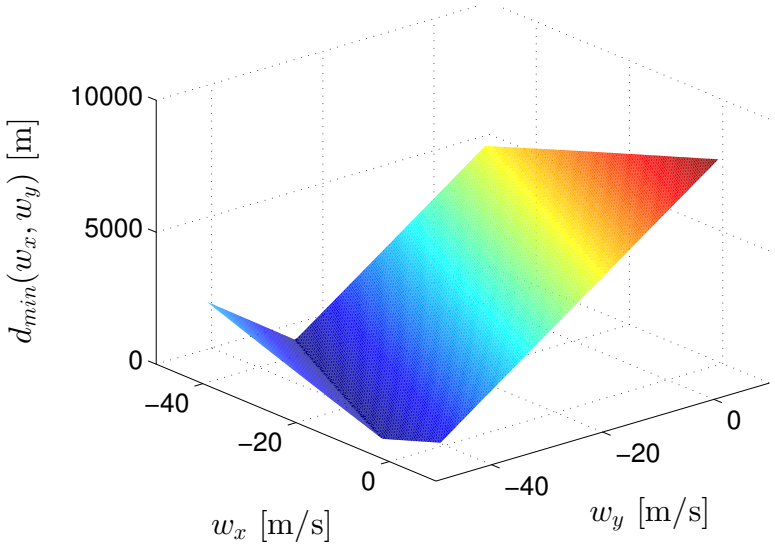

Figure 3.1 Example of a non-monotonic function: d_{min} for $\bar{w} = -20$m/s and $\delta_w = 25$m/s for a particular scenario.

To address the problem, one can divide the domain set R in $w_x w_y$ plane into n smaller ones R_j, where the transformation is one-to-one. Next, it is possible to compute the marginal PDFs in each of these n elements as

$$f_{y_1,j}(v_1) = \begin{cases} \int_{w_y} f_{v_1,w_y}(v_1, w_y) dw_y & w_x, w_y \in R_j \\ 0 & \text{otherwise} \end{cases} \tag{3.9}$$

The total density function is now obtained as a sum of the n PDFs functions, as follows.

$$f_{v_1}(v_1) = \sum_{j=1}^{n} f_{v_1,j}(v_1) \tag{3.10}$$

Let us use the aforementioned situation as an example. One can identify, as can be appreciated in Figure 3.1, two sets R_1 and R_2 where the function $d_{min}(w_x, w_y)$ is bijective, then compute $f_{d_{min},1}(d_{min})$ and $f_{d_{min},2}(d_{min})$ and finally obtain the total density function by adding these functions together.

3.1.2 Numerical approach

The numerical procedure used to solve the problem is addressed in this section. The computations herein described were performed using the numerical computing environment MATLAB.

The process is composed of three steps: the transformation of the function domain, computation of the joint probability f_{v_1,w_y} and integration over the auxiliary variable w_y.

Domain transformation

Firstly, in order to determine the limits of integration in equation (3.6) it is necessary to obtain the transformed domain set S in the $v_1 w_y$ plane from R in the $w_x w_y$ plane.

This is achieved by evaluating the function $v_1 = v_1(w_x, w_y)$ in the limits of the rectangular region in the $w_x w_y$ plane. Later, these points are interpolated in order to obtain a uniform grid over the variable v_1. This interpolation is performed using MATLAB's *interp1*.

An example of this transformation is depicted in Figure 3.2 for the variable $t_{d_{min}}$, a wind mean of $\bar{w}_x = \bar{w}_y = 0$m/s and a wind span of $\delta_{w_x} = \delta_{w_y} = 20$m/s in a given scenario. In this example, the transformation is one-to-one.

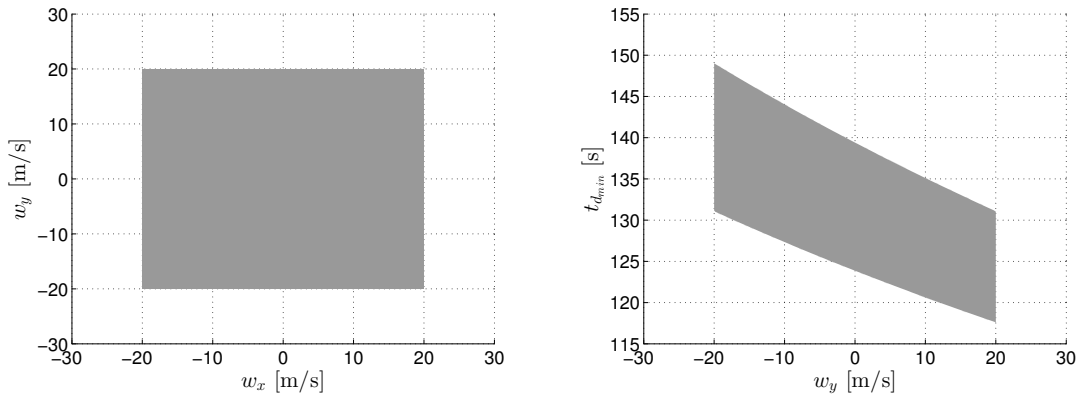

(a) R set. (b) S set.

Figure 3.2 Transformed domain for a one-to-one transformation.

For a non-monotonic function, it is also necessary to identify the points where the indicator function $v_1(w_x, w_y)$ reaches an extremum and define the separate regions where the joint probability function must be integrated. This has been accomplished by evaluating the function in a two-dimensional uniform grid in the $w_x w_y$ plane and then finding the function extrema using MATLAB's *max* and *min* functions in each dimension. Notice that it is possible for the functions to be monotonic for one wind direction and not for the other.

Once the limits of the regions R_j are found, the S_j sets in $v_1 w_y$ plane are computed by evaluating the function in these limits. The resulted points are now interpolated as done in the one-to-one transformation case.

In Figure 3.3 an example of a more-to-one domain transformation is presented. In this case, the variable Δt takes the place of Y and a wind span of $\delta_{w_x} = \delta_{w_y} = 50$m/s is used. In this scenario, it is necessary to separate the transformation into three disjoint regions R_1, R_2 and R_3 where the transformation is one-to-one. The function $\Delta t(w_x, w_y)$ maps these regions of the $w_x w_y$ plane into regions S_1, S_2 and S_3 of the $\Delta t w_y$ plane. Notice that region S_3 sightly overlaps region S_2.

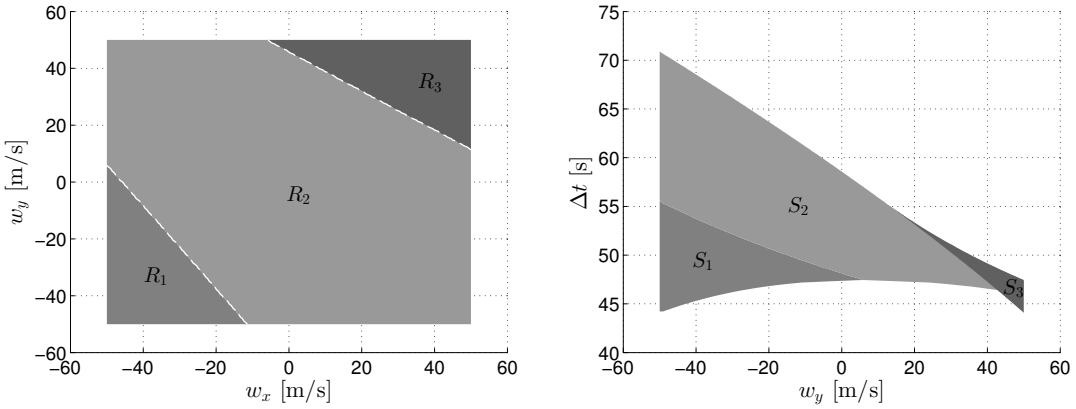

(a) R_j sets. (b) S_j sets.

Figure 3.3 Transformed domain for a more-to-one transformation.

Computation of the joint probability function

The next step is to compute the joint probability function f_{v_1,w_y}, which is given by

$$f_{v_1,w_y} = f_{w_x,w_y} \cdot \left| \frac{\partial w_x(v_1,w_y)}{\partial v_1} \right| \tag{3.11}$$

where f_{w_x,w_y} is the wind joint PDF (equation (2.22)). If one could obtain the analytical expressions of the inverse transformation $w_x(v_1,w_y)$ and its partial derivatives with respect of v_1, the computation of the joint PDF would be straightforward. However, the indicators herein defined do not allow to obtain such analytical expressions. These inverses, the partial derivatives, and the integrations are consequently computed numerically.

The inverse function $w_x(v_1,w_y)$ is obtained by applying MATLAB's functions *fzero* or *fsolve* to the following equation in w_x

$$z(w_x) = v_1(w_x,w_{y,0}) - v_{1,0} = 0 \tag{3.12}$$

where $v_{1,0}$ and $w_{y,0}$ are the points in which the function is evaluated. In the present problem, these points would be the ones in the S set (or sets).

In the cases where the indicator function is monotone in the R set, *fzero* is used. On the other hand, the function *fsolve* is used for the cases when the function its non-monotonic, that is to say, reaches an extremum in the R set.

The reason behind choosing one function or the other is that the function *fzero*, despite yielding more precise answers than *fsolve*, is incapable of finding a solution if the function does not present a sign change. For a non-monotonic function, *fzero* can present problems near the function extrema, where the function does not necessary cross the axis. In spite of the fact that the answer could not be as exact, the function *fsolve* does not have this problem near the extrema.

In both cases, it is necessary to provide an initial iteration point in w_x. Given that one already has a matrix $v_1(w_x,w_y)$ for a uniform grid in w_x,w_y (necessary to compute the transformed domains), this initial guess is obtained by interpolating the matrix in the $v_{1,0}$ and w_{y_0} points using MATLAB's *interp2* and *interp1*. This way, a very accurate $w_{x,0}$ initial point is obtained.

Once the inverse function is computed, the partial derivative can be obtained by applying the following finite difference formula

$$\frac{\partial w_x(v_1,w_y)}{\partial y} \approx \frac{w_x(v_1+h,w_y) - w_x(v_1-h,w_y)}{2h} \tag{3.13}$$

where the step h is chosen as

$$h = v_{1,c}\sqrt{\varepsilon(v_{1,c})} \tag{3.14}$$

expression where ε stands for the machine accuracy, obtained using *eps* function, and $v_{1,c}$ is a characteristic value of the indicator.

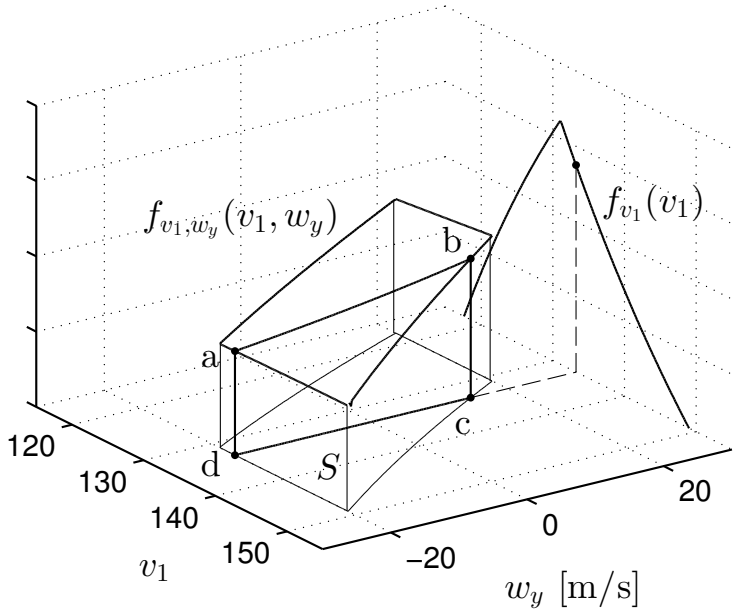

Figure 3.4 Joint and marginal probability functions.

Integration over $\mathbf{w_y}$

Finally, the joint PDF is integrated over w_y to obtain the marginal PDF $f_{v_1}(v_1)$.

For each point of the uniform grid in the variable v_1, the joint PDF is integrated inside the limits of the S set. In this project, MATLAB's function *trapz* has been used.

In Figure 3.4 a representation of the procedure is depicted. Once the joint PDF f_{v_1,w_y} is computed over the S set, one can obtain the marginal PDF for a point in v_1 by integrating over w_y inside the limits defined by S: in the picture, the magnitude of the area *abcd* represent this integration.

3.2 Monte Carlo Method

In this Section, the application of the Monte Carlo method to the problem is addressed. The results compiled using these simulations are to be used as a validation of the ones obtained with the transformation of variables analysis.

The Monte Carlo method is based on repeatedly evaluating a deterministic model using a random sampling as an input, in order to generate a random output from which one can obtain statistical data such as the mean, variance or the probability distribution.

This method is based on the *Law of Large Numbers*, which states that, given independent and identically distributed random variables (*i.i.d*) $X_1, X_2, \ldots, X_N$, then the average

$$\bar{X} = \frac{1}{N}\sum_{i=1}^{N} X_i \tag{3.15}$$

converges to $E[X]$ when N tends to infinity.

The main limitation of this method is that a large number of samples is necessary to obtain a desired accuracy, and the model equations have to be evaluated for each sample. On the other hand, the Monte Carlo method has the advantage of being very flexible in the complexity of the model: since this model is only used as a simulator, it is possible to obtain solutions to problems that are too difficult to be solved analytically.

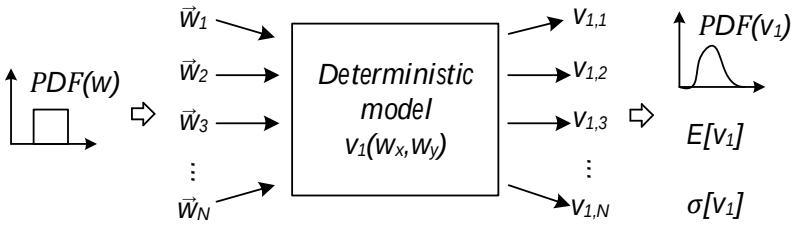

Figure 3.5 Basics of Monte Carlo method.

Taking this into consideration, it is necessary to reach a trade-off between the computational effort and the accuracy of the solution.

The Monte Carlo method can be applied to the problem considered in this project to obtain statistical information of the indicators from a random sample of wind velocities $\vec{w}_k$.

The method is applied to the problem as follows.

From the uniform wind distribution defined in equation (2.20), a set of N samples $\{w_{x,k}, w_{y,k}\}$ is generated using MATLAB's *rand* function. These samples are used to solve the indicator equations described in 2.2 to obtain a sample of the solution $\{v_{1,k}\}$.

Once the N samples of the output are generated, these data can be used to find approximate values of the mean and the typical deviation:

$$\bar{v}_1 = \frac{1}{N}\sum_{k=1}^{N} v_{1,k} \tag{3.16}$$

$$\sigma = \sqrt{\frac{1}{N-1}\sum_{k=1}^{N} |v_{1,k} - \bar{v}_1|^2} \tag{3.17}$$

These values are obtained using MATLAB's *mean* and *std* functions.

Additionally, an approximation to the indicator PDF can be computed from the data by normalizing their *histogram*. In order to do so, the output data is divided into a series of adjacent intervals (or *bins*) of equal size. Then, the number of values that fall into each interval is counted and stored in a vector n_{v_1} of size M, being M the number of bins. An approximation in M points of the sought PDF can now be computed as

$$f_{v_1} = \frac{n_{v_1}}{Nd} \tag{3.18}$$

where N is the size of the sample in the simulation and d is the size of each bin. This procedure has been carried out using the function *hist* in MATLAB.

3.2.1 Number of samples

As it has been stated, the size of the input sample N defines the quality of the solution in Monte Carlo simulations. In consequence, it is important to chose N sufficiently large so that the solution is accurate enough.

Table 3.1 Approximate error in a Monte Carlo simulation.

N	$\varepsilon[t_{d_{min}}]$	$\varepsilon[d_{min}]$	$\varepsilon[\Delta t]$
$2^9 = 512$	0.6967s	122.4334m	1.7979s
$2^{16} = 65536$	0.0642s	10.8240m	0.1606s
$2^{23} = 8388608$	0.0057s	0.9564m	0.0142s

According to Bayer et al. [2], the accuracy of the approximation can be characterized by the probability that the error of the mean obtained by the Monte Carlo simulation is larger than certain tolerance ε. This can be estimated as

$$P[|\bar{v}_1 - E[v_1]| > \varepsilon] \approx 2\left(1 - \Phi\left[\frac{\sqrt{N}\varepsilon}{\sigma[v_1]}\right]\right) \tag{3.19}$$

where $E[v_1]$ is the true mean of the random variable and Φ stands for the standard normal cumulative distribution function.

Let us consider the same scenario used in the example for Figure 3.2. In Table 3.1, the errors ε of approximating the mean of the variables $t_{d_{min}}$, d_{min} and Δt for a probability of $P[|\bar{v}_1 - E[v_1]| > \varepsilon] = 1\%$ are presented for $N = 2^9$, $N = 2^{16}$ and $N = 2^{16}$. It can be observed that for the larger sample one obtains a very good approximation for all indicators.

In Figure 3.6, the PDF of the variable $t_{d_{min}}$ is depicted for the aforementioned sample sizes. In this picture, it is easy to appreciate the importance of using a sufficiently large number of samples.

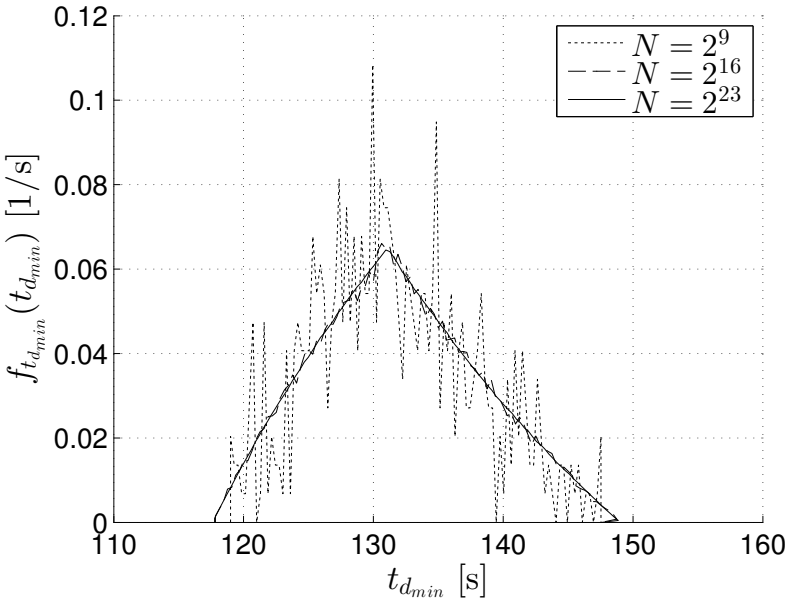

Figure 3.6 Time to minimum distance PDF for different number of samples in a Monte Carlo simulation.

Taking all of this into account, a number of samples of $N = 2^{23} = 8.4 \cdot 10^6$ has been chosen for carrying out all Monte Carlo simulations presented throughout this project.

4 Results

In this chapter, the obtained results are presented for two different scenarios. The influence of parameters such as the mean wind $\bar{w}$, the wind span δ_w and the aircraft airspeed V is analysed.

The results are presented for two particular scenarios and a uniform wind distribution whose PDF is defined in (2.20). It has been decided to use the same PDF for both wind components w_x and w_y, that is

$$\bar{w}_x = \bar{w}_y = \bar{w} \qquad \delta_{w_x} = \delta_{w_y} = \delta_w \tag{4.1}$$

Positive values of $\bar{w}$ represent that on average the wind points north-east while positive values represent a wind that points south-west. The mean value $\bar{w}$ varies between -20m/s and 20m/s and the wind span ranges from 0m/s (representing the deterministic scenario) to 25m/s.

The airspeeds are also equal for both aircraft $V_A = V_B = V$. Values between 200m/s and 280m/s are considered. The separation requirement D is set to 5NM (9260m).

4.1 Conflict scenarios

The two particular scenarios under consideration are described in this section. In Figure 4.1, the initial positions $\vec{s}_{0,i}$ and courses ψ_i for aircraft A and B are depicted. These parameters are set to the following values:

- **Scenario 1:** $\vec{s}_{0,A} = [0,0]$, $\vec{s}_{0,B} = [10,10]$NM$= [18520, 18520]$m, $\psi_A = 90^\circ$ and $\psi_B = 135^\circ$
- **Scenario 2:** $\vec{s}_{0,A} = [0,0]$, $\vec{s}_{0,B} = [25,50]$NM$= [46300, 92600]$m, $\psi_A = 90^\circ$ and $\psi_B = 225^\circ$

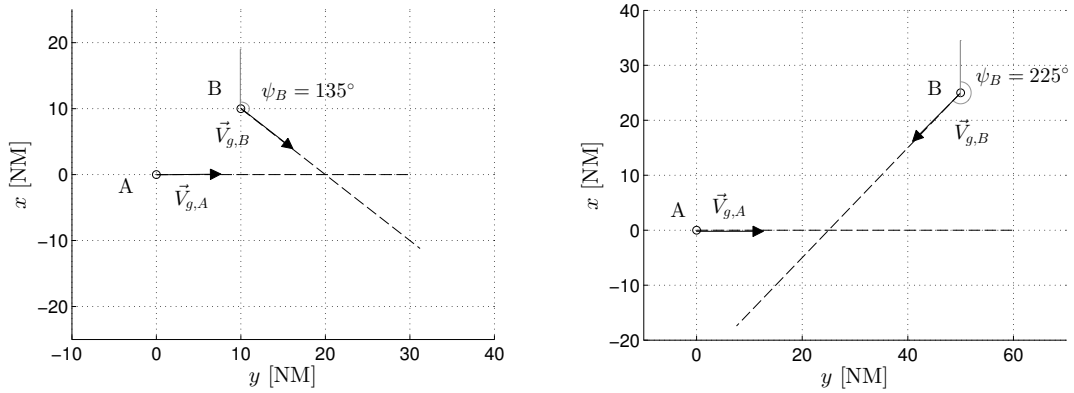

(a) Scenario 1.

(b) Scenario 2.

Figure 4.1 Conflict scenarios.

4.1.1 Deterministic analysis

Next, the results of a simple deterministic analysis are presented. The equations described in section 2.2 have been evaluated for a known wind, that is to say, $\delta_w = 0$.

The indicators have been computed for a nil wind mean ($\bar{w} = 0$) and aircraft airspeeds of $V = 240$m/s. In Table 4.1, the results are presented for scenarios 1 and 2.

Table 4.1 Deterministic analysis results.

	$t_{d_{min}}$	d_{min}	Conflict	Δt
Scenario 1	131.73s	10022.95m (5.41NM)	No	-
Scenario 2	232.87s	7339.14m (3.96NM)	Yes	25.46s

In the first scenario, the deterministic analysis predicts a minimum distance between aircraft slightly greater than the separation requirement, so no conflict is detected. However, since this minimum distance is close to D, one may expect the existence of a conflict for certain wind configurations.

For the situation described in the second scenario, the deterministic analysis predicts a loss of separation with a duration of 25.46 seconds. The time to minimum distance in this situation is greater than the obtained in the first scenario, which is easily explained by the fact that the initial distance between the aircraft is bigger in the second one (55.90NM versus 14.14NM).

These results give an idea of the behaviour of the overall situation for each scenario; in the following sections, an uncertain wind is considered.

4.2 Aircraft relative distance over time

The results regarding the distance between the two aircraft over time are now presented considering the following wind and airspeed parameters: $\bar{w} = 0$m/s, $\delta_w = 20$m/s and $V = 240$m/s.

The expected value $E[d(t)]$ (solid), 5th percentile (dashed) and 95th percentile (doted) of the variable have been depicted in Figure 4.2, where the dashed-doted line represents the minimum horizontal separation requirement D. For the sake of clarity, the results obtained by means of a Monte Carlo simulation are not shown in this picture.

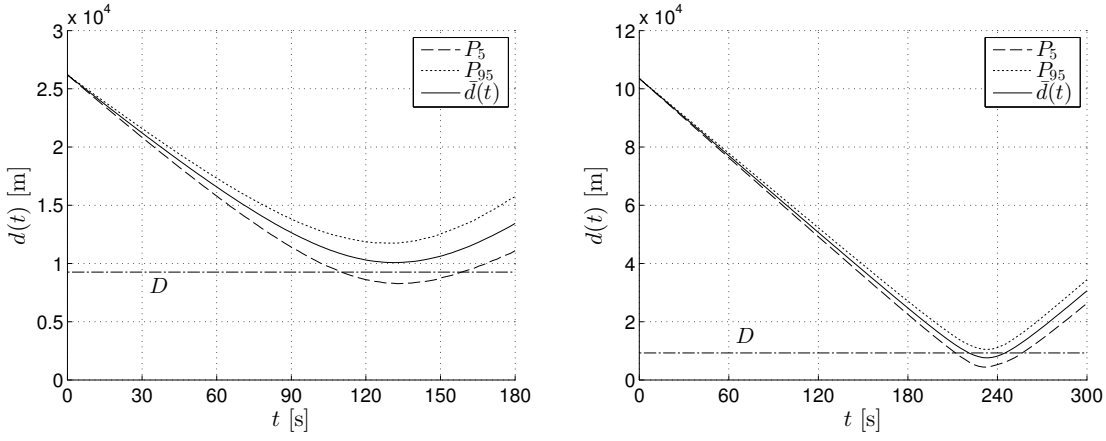

(a) Scenario 1.

(b) Scenario 2.

Figure 4.2 Distance between the aircraft over time using transformation of variables.

Since the aircraft are approaching, the relative distance between them decreases until it reaches a minimum, and then increases as the aircraft move away from each other.

As one may expect, the uncertainty of the aircraft distance increases with time. For reference, the standard deviation of this magnitude goes from zero at the beginning to $\sigma[d(180)] = 1462.8$m (1463.1m using a

Monte Carlo simulation) in the first scenario, and $\sigma[d(180)] = 1469.1$m in the second one (1469.5m with Monte Carlo method).

An interesting feature shown in this picture is the assurance that the existence of loss of separation at a given time is uncertain. For instance, in scenario 1 at $t = 110$s, where the separation minima line crosses the 5th percentile, the aircraft have a 5% probability of being in a loss of separation.

4.3 Time to minimum distance

Probability distribution

The probability density function of the indicator $t_{d_{min}}$ is now analysed for $\bar{w} = 0$m/s, $\delta_w = 20$m/s and $V = 240$m/s. In Figure 4.3 the transformed two-dimensional set S and PDFs for this variable are presented for scenarios 1 (Figure 4.3 (a) and (b)) and 2 (Figure 4.3 (c) and (d)). From now on, the results are shown for both transformation of variables (solid) and Monte Carlo (dashed) methods.

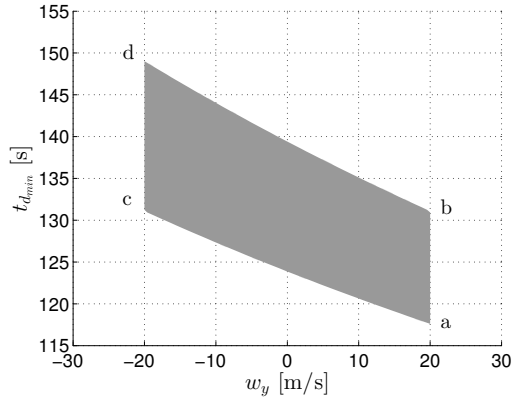

(a) S set in the $t_{d_{min}} w_y$ plane for scenario 1.

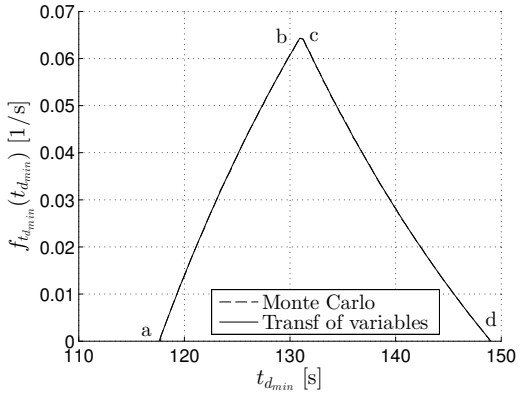

(b) PDF of $t_{d_{min}}$ for scenario 1.

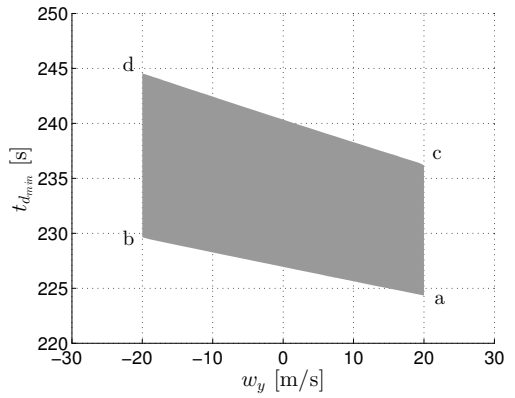

(c) S set in the $t_{d_{min}} w_y$ plane for scenario 2.

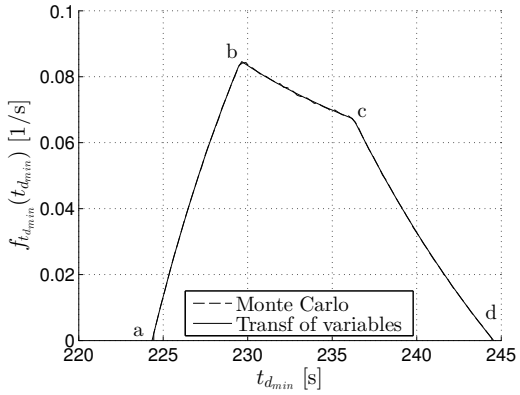

(d) PDF of $t_{d_{min}}$ for scenario 2.

Figure 4.3 Transformed domain and probability distribution of $t_{d_{min}}$ for $\bar{w} = 0$m/s, $\delta_w = 20$m/s and $V = 240$m/s..

The PDFs of $t_{d_{min}}$ present four corners (labeled as a, b, c and d in Figure 4.3). This can be explained by the presence of the four corners in the S sets, which represent abrupt changes in the integration limits when integrating the joint PDF $f_{t_{dmin},w_y}(t_{d_{min}}, w_y)$ to obtain the marginal PDF.

In the first scenario, two of these corners (b and c, at $t_{d_{min}} = 130.9$s and $t_{d_{min}} = 131.3$s respectively) are very close to each other and are difficult to differentiate. The difference in height of the middle corners b (229.6s) and c (236.2s) in the second scenario responds to different values of the partial derivative $\partial w_x / \partial t_{dmin}$ at these points, since the limits of integration in w_y remain the same.

In Table 4.2, the mean and standard deviation values of $t_{d_{min}}$ are collected. Both transformation of variables and Monte Carlo methods yield very similar results. Notice that the expected value of t_{dmin} for both scenarios

Table 4.2 Expected value and standard deviation of $t_{d_{min}}$.

	Scenario 1		Scenario2	
Method	$E[t_{d_{min}}]$	$\sigma[t_{d_{min}}]$	$E[t_{d_{min}}]$	$\sigma[t_{d_{min}}]$
Transformation of variables	131.87s	6.38s	233.11s	4.33s
Monte Carlo	131.89s	6.38s	233.14s	4.33s

is slightly bigger than the time obtained with a deterministic analysis using the average wind $\bar{w} = 0$m/s, 131.73s.

Effect of the wind uncertainty

The effects of the parameters $\bar{w}$ and δ_w are analysed in this section for $V = 240$m/s. Figure 4.4 depicts the expected value $E[t_{d_{min}}]$ and the standard deviation $\sigma[t_{d_{min}}]$ as a function of $\bar{w}$ for different values of the wind width $\delta_w = 5, 10, 15, 20$ and 25m/s.

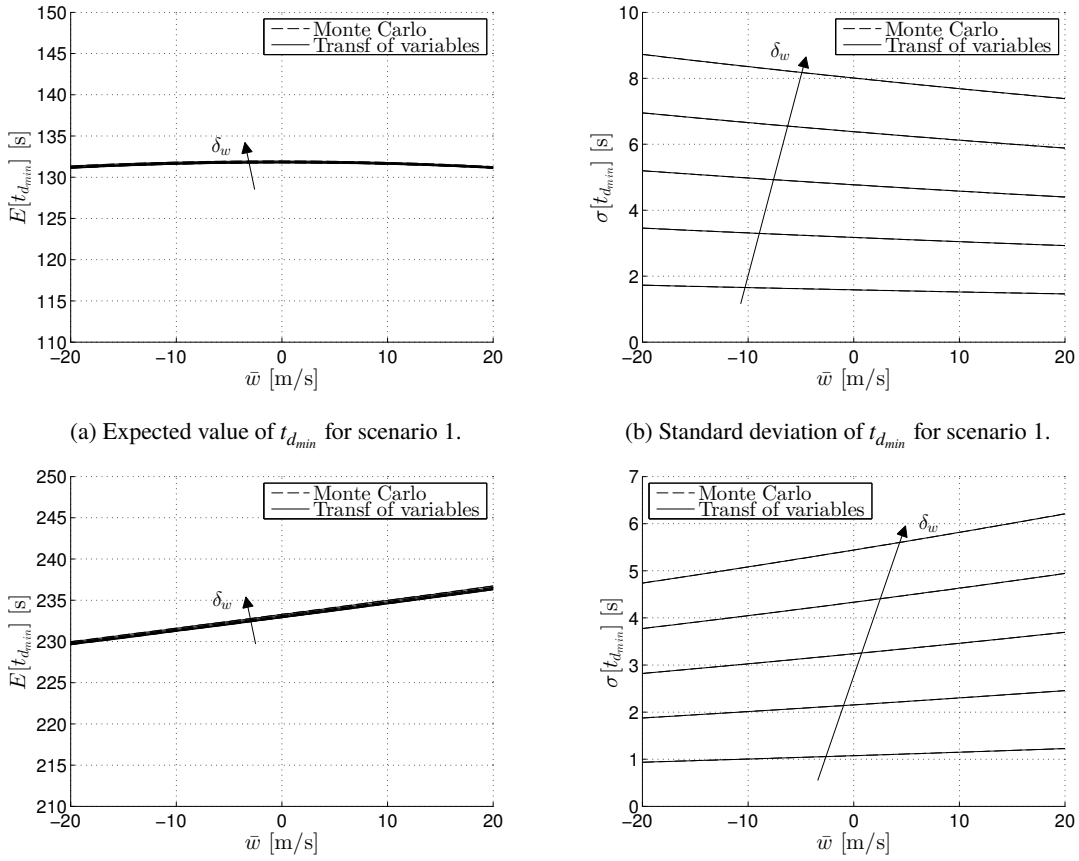

(a) Expected value of $t_{d_{min}}$ for scenario 1.

(b) Standard deviation of $t_{d_{min}}$ for scenario 1.

(c) Expected value of $t_{d_{min}}$ for scenario 2.

(d) Standard deviation of $t_{d_{min}}$ for scenario 2.

Figure 4.4 Expected value and standard deviation of $t_{d_{min}}$ as a function of $\bar{w}$, for $\delta_w = 5, 10, 15, 20, 25$m/s and $V = 240$m/s.

As one can observe in the picture, in both scenarios the expected value of $t_{d_{min}}$ is almost independent on δ_w; it increases very slightly when δ_w does. The expected value also depends very briefly on the wind mean: the influence of $\bar{w}$ on $E[t_{d_{min}}]$ is basically non-existent in scenario 1, while in the second scenario the expected value increases as the mean wind does. The reason behind this increase in $E[t_{d_{min}}]$ is that larger values of $\bar{w}$ represent stronger north-east winds, which for the aircraft B (see Figure 4.1) translate into headwinds that will delay the loss of separation between the two aircraft.

Regarding the standard deviation of $t_{d_{min}}$, it depends weakly on $\bar{w}$, decreasing slightly on scenario 1 and increasing in scenario 2. As one may expect, the standard deviation increases as δ_w increases, that is to say, a bigger dispersion in wind values translates to a bigger dispersion in $t_{d_{min}}$. As a reference, when δ_w increases 1m/s, the standard deviation at $\bar{w} = 0$ increases approximately 0.3s and 0.2s for scenarios 1 and 2, respectively.

Effect of the aircraft airspeeds

In this section, the effect of the aircraft velocities V on $t_{d_{min}}$ is presented. In Figure 4.5 the expected value $E[t_{d_{min}}]$ and the standard deviation $\sigma[t_{d_{min}}]$ as a function of V are represented for $\bar{w} = 0$m/s and $\delta_w = 5, 10, 15, 20, 25$m/s.

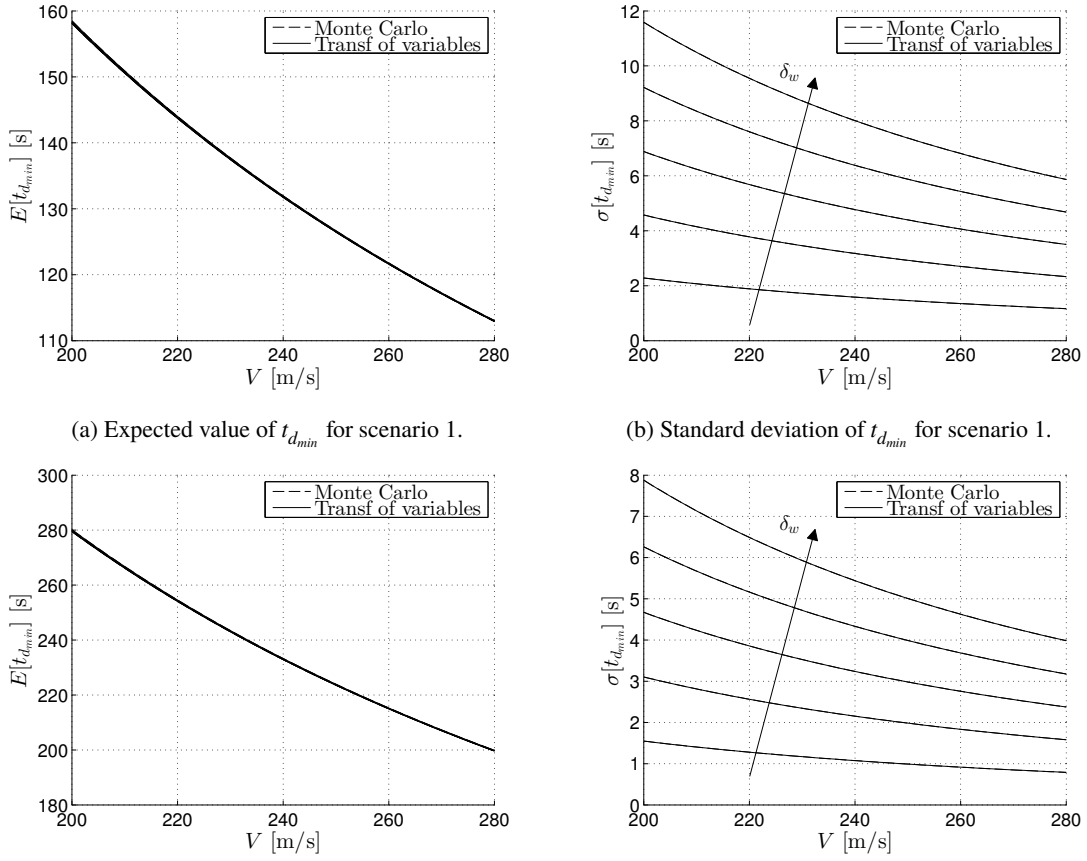

(a) Expected value of $t_{d_{min}}$ for scenario 1.

(b) Standard deviation of $t_{d_{min}}$ for scenario 1.

(c) Expected value of $t_{d_{min}}$ for scenario 2.

(d) Standard deviation of $t_{d_{min}}$ for scenario 2.

Figure 4.5 Expected value and standard deviation of $t_{d_{min}}$ as a function of V, for $\bar{w} = 0$ and $\delta_w = 5, 10, 15, 20, 25$m/s and $V = 240$m/s.

The effect of V is very similar in both scenarios. The expected value of $t_{d_{min}}$ decreases as the airspeed increases, a predictable result that shows how the aircraft approach each other faster when their airspeeds increase.

The interesting feature about the present result is that the standard deviation decreases when V increases, and this change is more significant for higher values of δ_w. For example, in scenario 1, when the airspeed increases from 200m/s to 280m/s the standard deviation decreases approximately 1s for $\delta_w = 5$m/s and 6s for $\delta_w = 25$m/s; for scenario 2, $\sigma[t_{d_{min}}]$ decreases 0.8s and 4s for $\delta_w = 5$ and 25m/s, respectively. This behaviour can be explained by equation (2.19): since the aircraft airspeed are dividing the crosswinds, which are the source of uncertainty, it is expected that bigger values of V would translate into a more certain trajectory.

4.4 Minimum distance

Probability distribution

Next, the density function of the minimum distance d_{min} between aircraft is presented for the two scenarios and $\bar{w} = 0$, $\delta_w = 20$m/s, $V = 240$m/s. The results are depicted in Figure 4.6, where the S sets for each scenario are also represented.

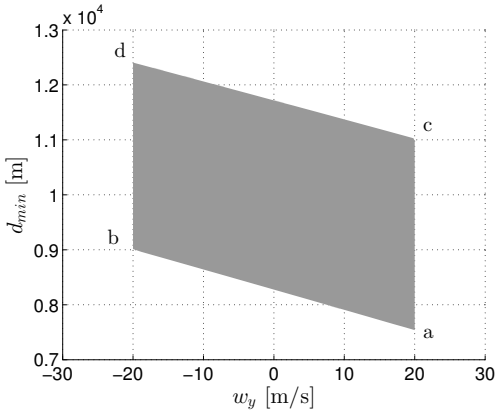

(a) S set in the $d_{min}w_y$ plane for scenario 1.

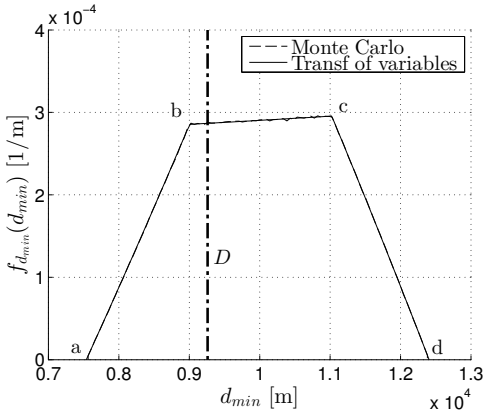

(b) PDF of d_{min} for scenario 1.

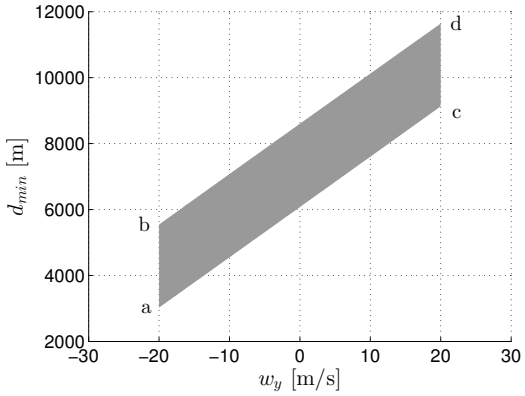

(c) S set in the $d_{min}w_y$ plane for scenario 2.

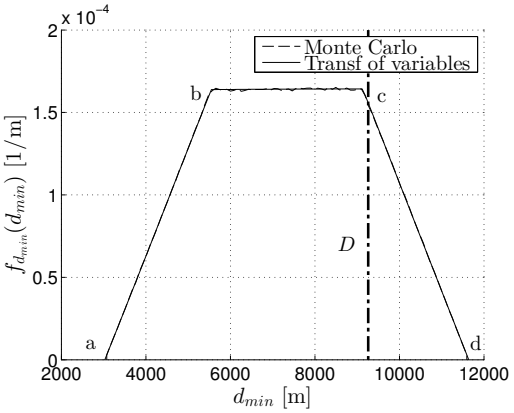

(d) PDF of d_{min} for scenario 2.

Figure 4.6 Transformed domain and probability distribution of d_{min}, for $\bar{w} = 0$m/s, $\delta_w = 20$m/s and $V = 240$m/s.

The probability of conflict can be computed from these PDFs by obtaining the area under the function to the left of the vertical dash-doted line that represents the minimum separation criterion D:

$$P_{con} = \int_{-\infty}^{D} f_{d_{min}}(\rho) d\rho \tag{4.2}$$

The presented PDFs display again four corners, which, as in the case of $t_{d_{min}}$, can be explained by the four corners of the transformed domains.

Notice that the points a, b, c and d in these functions are almost connected by straight lines, unlike the case of $t_{d_{min}}$, where some curvature exists. This fact clearly shows that the shape of the PDF of d_{min} is highly influenced by the shape of the set S and not so much by the value of the Jacobian of the transformation, which seems to be quite constant in the whole region. This is also the reason why the points b and c have the same height, which is mostly affected by the values of the limits of integration.

The obtained values of $E[d_{min}]$, $\sigma[d_{min}]$ and P_{con} are collected in Table 4.3 for transformation of variables and Monte Carlo methods. Once more, the results differ little from one method to the other.

Table 4.3 Expected value, standard deviation of d_{min} and probability of conflict.

	Scenario 1			Scenario2		
Method	$E[d_{min}]$	$\sigma[d_{min}]$	P_{con}	$E[d_{min}]$	$\sigma[d_{min}]$	P_{con}
Transformation of variables	10012.4m	1075.6m	27.98%	7337.6m	1902.3m	81.48%
Monte Carlo	10013.0m	1075.2m	27.95%	7337.6m	1903.9m	81.49%

Effect of the wind uncertainty

In this section, the effects of $\bar{w}$ and δ_w on the minimum distance expected value and standard deviation are studied for $V = 240$m/s. The results are depicted as a function of $\bar{w}$ in Figure 4.7 for $\delta_w = 5, 10, 15, 20$ and 25m/s.

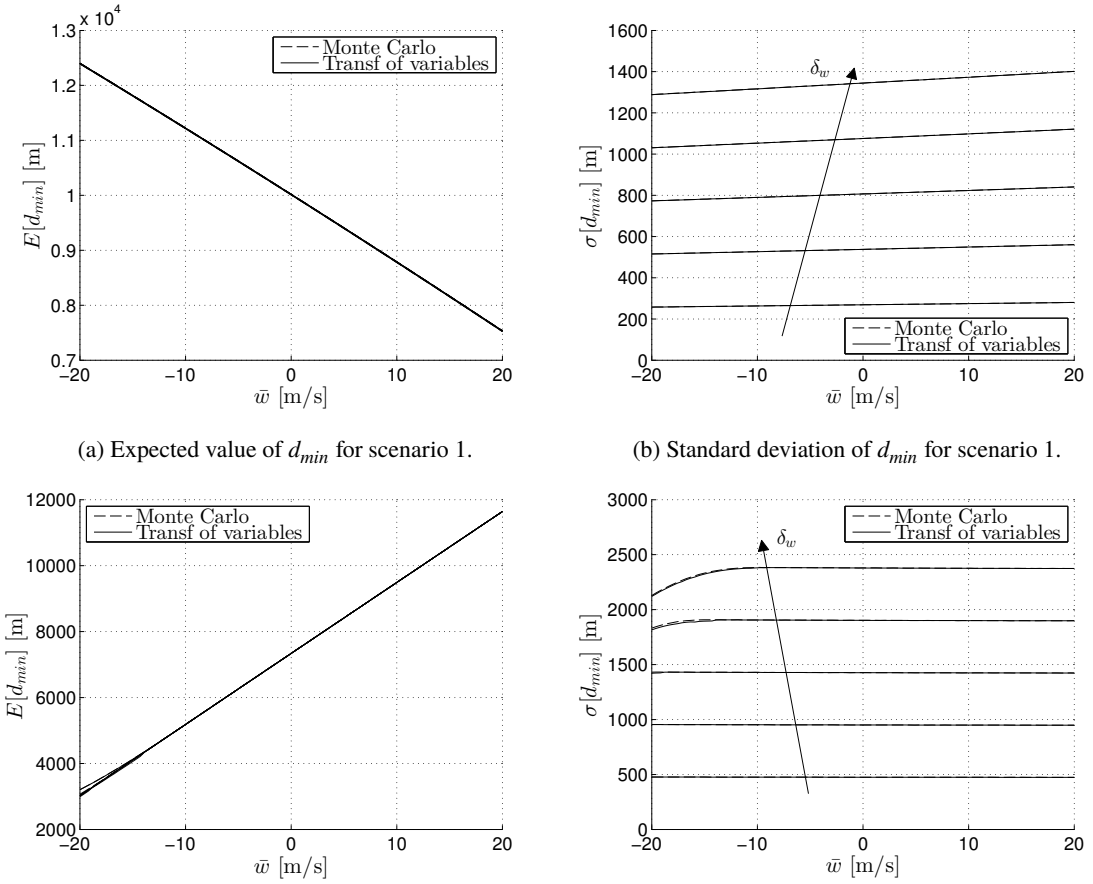

(a) Expected value of d_{min} for scenario 1.

(b) Standard deviation of d_{min} for scenario 1.

(c) Expected value of d_{min} for scenario 2.

(d) Standard deviation of d_{min} for scenario 2.

Figure 4.7 Expected value and standard deviation of d_{min} as a function of $\bar{w}$, for $\delta_w = 5, 10, 15, 20, 25$m/s and $V = 240$m/s.

Again, the expected value of the indicator does not depend on the wind PDF width. However, unlike the case of $t_{d_{min}}$, the wind mean has a relevant influence in this indicator: for scenario 1, the expected value decreases as $\bar{w}$ increases; for scenario 2, the opposite trend appears.

This can be explained considering the deterministic case: as $\bar{w}$ increases, the wind goes from pointing south-west to pointing north-east; in consequence, the aircraft airspeeds rotates clockwise to keep their course constant, which affects aircraft B more because the wind direction is perpendicular to its course. As a result, the relative ground speed V_g also rotates clockwise and becomes more aligned with the relative initial position vector $\vec{s}_0$. This causes the term $(\vec{s}_0.\vec{V}_g)^2/V_g^2$ in equation (2.6) to increase and, consequently, d_{min} decreases.

In scenario 2, the course of the aircraft B is parallel to the wind direction. While for aircraft A the previous analysis predicts its airspeed to rotate, the aircraft B airspeed does not rotate in this case, but increases its value when $\bar{w}$ increases. It can be checked that in this scenario the vector $\vec{V}_g$ is more perpendicular to $\vec{s}_0$ as $\bar{w}$ increases, which causes the term $(\vec{s}_0.\vec{V}_g)^2/V_g^2$ to decrease and, as a result, the minimum distance between aircraft increases.

As can be observed in the figure, the wind mean has almost no effect on the standard deviation of d_{min}, which slightly increases with $\bar{w}$ for the first scenario and remains constant in scenario 2 for $\delta_w = 5, 10$ and 15m/s. Once again, the standard deviation of the indicator increases as δ_w increases.

The interesting result obtained in this analysis appears when one observes the behaviour of $\sigma[d_{min}]$ for values of $\bar{w}$ near -20m/s and high values of δ_w in the second scenario: the standard deviation of the minimum distance drops for these values. While this is more striking for the standard deviation, it can also be observed for $E[d_{min}]$ near $\bar{w} = -20$m/s, where the expected value for $\delta_w = 25$m/s is higher than the others.

The reason behind this behaviour is that the function $d_{min}(w_x, x_y)$ reaches a minimum ($d_{min} = 0$m, which can be understood as a collision between the aircraft) for some values of the wind speed that are predicted by its PDF. In the context of the transformation of variables method, this will mean that the domain separation into two disjoints regions is necessary.

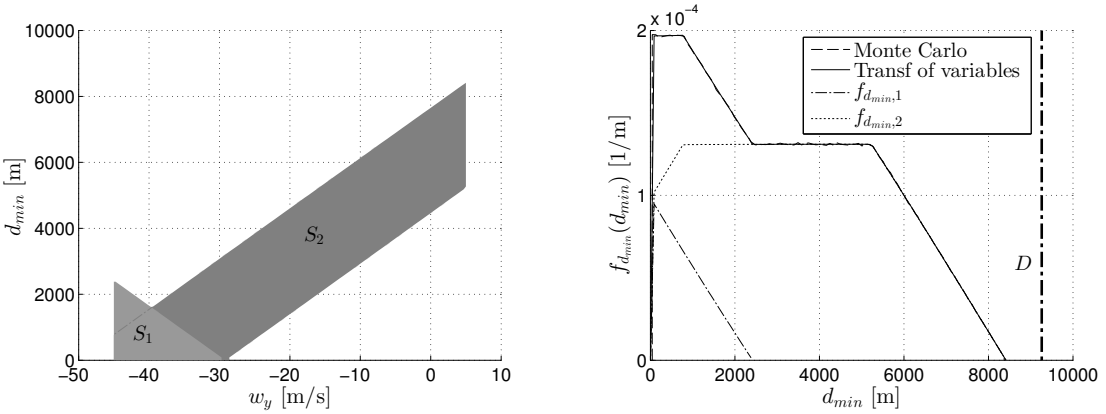

(a) S_1 and S_2 sets in the $d_{min}w_y$ plane.

(b) PDF of d_{min}.

Figure 4.8 Transformed domains and probability distribution of d_{min} for scenario 2, $\bar{w} = -20$m/s, $\delta_w = 25$m/s and $V = 240$m/s.

In Figure 4.8 (a), the transformed sets S_1 and S_2 are depicted for $\bar{w} = -20$m/s, $\delta_w = 25$m/s and $V = 240$m/s; as can be seen, the S_1 set partially overlaps S_2 set. In Figure 4.8 (b) the obtained PDF is represented. The contribution of each set to the total PDF are presented in this picture as $f_{d_{min},1}$ (dash-doted) and $f_{d_{min},2}$ (doted).

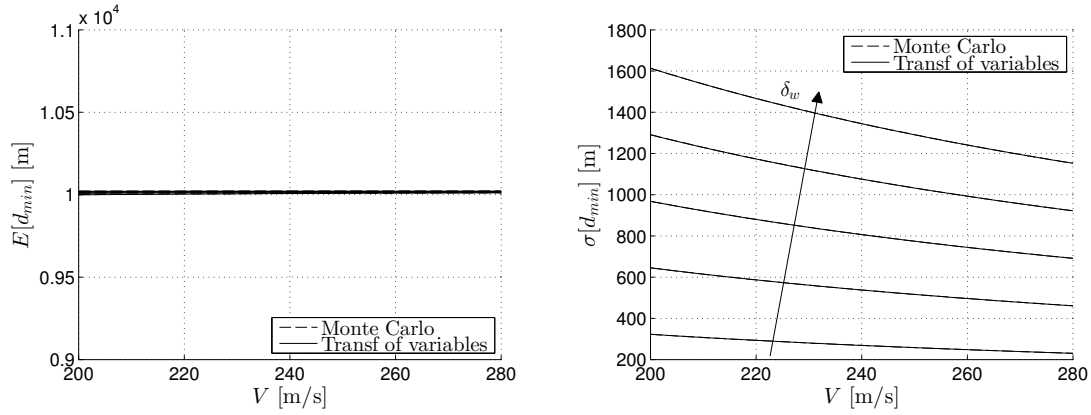

(a) Expected value of d_{min} for scenario 1.

(b) Standard deviation of d_{min} for scenario 1.

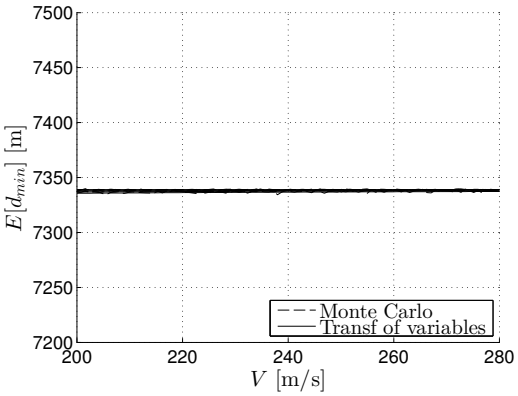

(c) Expected value of d_{min} for scenario 2.

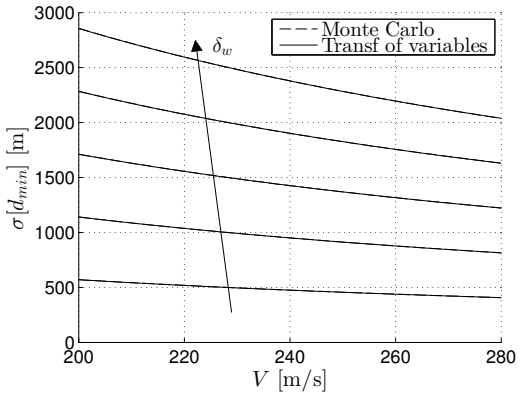

(d) Standard deviation of d_{min} for scenario 2.

Figure 4.9 Expected value and standard deviation of d_{min} as a function of V, for $\bar{w} = 0$m/s and $\delta_w = 5, 10, 15, 20, 25$m/s.

As it can be seen in the this figure, in this situation the PDF of d_{min} is higher around $d_{min} = 0$m. This causes the PDF to be narrower and, in consequence, the standard deviation to be smaller.

Effect of the aircraft airspeeds

The effects of the aircraft airspeeds in d_{min} are addressed in this section. The expected value and standard deviation are depicted in Figure 4.9 for $\bar{w} = 0$m/s and $\delta_w = 5, 10, 15, 20$ and 25m/s.

Aircraft airspeeds have no impact on the expected value of d_{min} whatsoever. The wind span δ_w also has no influence on this parameter. The behaviour of $\sigma[d_{min}]$ is exactly the same as in $t_{d_{min}}$ case: the standard deviation decreases with V, being this reduction more important for higher values of δ_w.

4.5 Probability of being in loss of separation at a given distance

The probability for an aircraft to be in a loss of separation for each point of its trajectory is analysed next. The results herein presented are computed for the aircraft A. For aircraft B, the existence of a loss of separation takes place in an earlier point of the trajectory in comparison to aircraft A for the first scenario, whereas in the second scenario, the loss of separation for aircraft B starts later. In spite of this fact, the results are very similar for both aircraft.

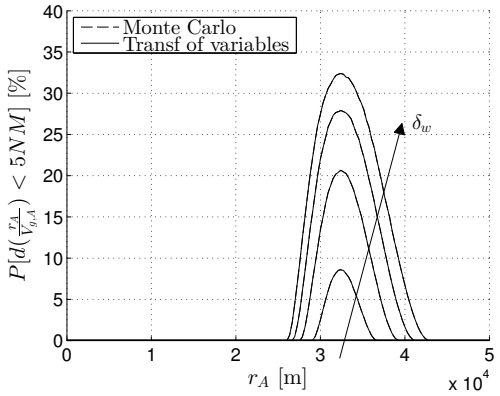

(a) $P[d(r_A/V_{g,A} \leq 5NM)]$ for scenario 1.

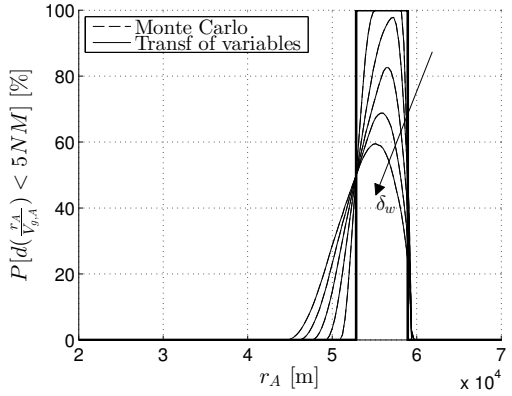

(b) $P[d(r_A/V_{g,A} \leq 5M)]$ for scenario 2.

Figure 4.10 Probability for aircraft A of being in loss of separation $P[d(r_A/V_{g,A} \leq 5NM)]$ as a function of r_A, for $\bar{w} = 0$, $\delta_w = 0, 5, 10, 15, 20, 25$m/s and $V = 240$m/s.

In Figure 4.10, the probability for the aircraft A of being in a loss of separation $P[d(r_A/V_{g,A} \leq 5NM)]$ as a function of the aircraft position along its trajectory r_A is depicted for $\bar{w} = 0$, $V = 240$m/s and different values of δ_w: $\delta_w = 0, 5, 10, 15, 20$ and 25m/s. The value $\delta_w = 0$m/s corresponds to a deterministic analysis, and is represented in the figure with a thicker line.

In both scenarios, the probability is zero at the beginning and starts to grow from a certain value of the aircraft distance. Then, it reaches a maximum and descends, so it becomes zero again as the two aircraft move away from each other.

For the first scenario, the deterministic analysis ($\delta_w = 0$m/s) predicts no loss of separation along the whole trajectory. However, for uncertain winds a probability of a loss of separation appears: as the wind PDF width δ_w increases, the probability of a loss of separation increases for values of r_A around 30km. The maximum probability appears approximately at 32km, with a value of 32% for $\delta_w = 25$m/s.

In the second scenario, a loss of separation between $r_A = 52.8$km and $r_A = 58.9$km is predicted in the deterministic analysis. The probability of being in loss of separation increases with δ_w outside this region and decreases inside it. This is a very interesting result that will also be seen later in section 4.6: The certainty that a loss of separation exists or does not exist decreases as the wind uncertainty increases.

Next, in Figure 4.11, the effects of the mean wind $\bar{w}$ are analysed for $\delta_w = 20$m/s and $V = 240$m/s. Values of $\bar{w} = -20, -10, 0, 10$ and 20m/s are considered.

In this case, the probability of being in loss of separation increases when the wind mean increases for scenario 1, while in scenario 2, the probability decreases when $\bar{w}$ increases. This can be easily explained by

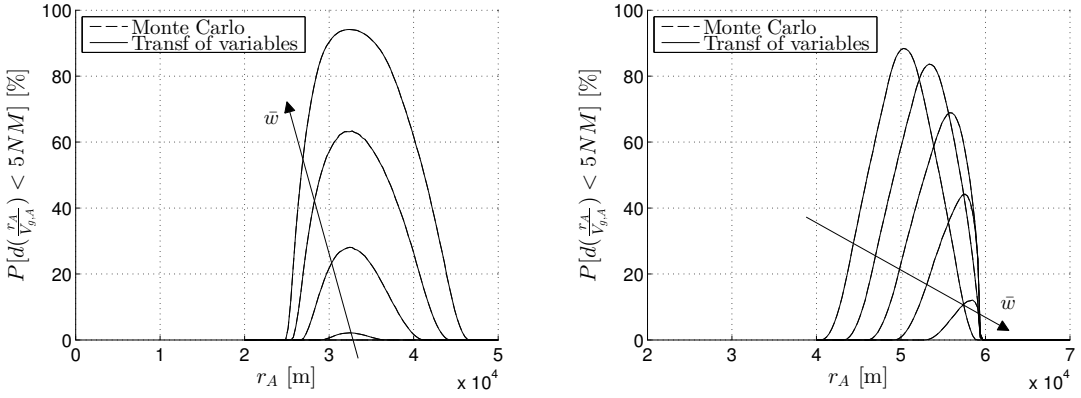

(a) $P[d(r_A/V_{g,A} \leq 5NM)]$ for scenario 1.

(b) $P[d(r_A/V_{g,A} \leq 5NM)]$ for scenario 2.

Figure 4.11 Probability for aircraft A of being in loss of separation $P[d(r_A/V_{g,A} \leq 5NM)]$ as a function of r_A, for $\bar{w} = -20, -10, 0, 10, 20$m/s, $\delta_w = 20$m/s and $V = 240$m/s.

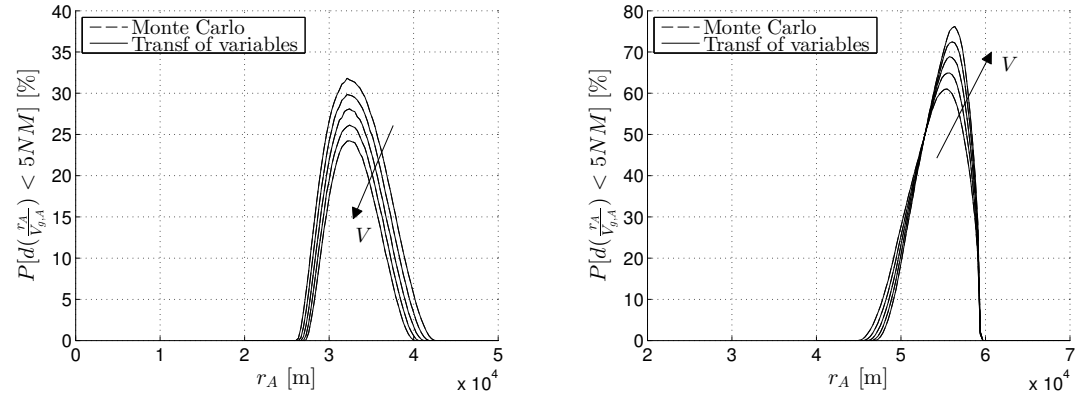

(a) $P[d(r_A/V_{g,A} \leq 5NM)]$ for scenario 1.

(b) $P[d(r_A/V_{g,A} \leq 5NM)]$ for scenario 2.

Figure 4.12 Probability for aircraft A of being in loss of separation $P[d(r_A/V_{g,A} \leq 5NM)]$ as a function of r_A, for $\bar{w} = 0$m/s, $\delta_w = 20$m/s and $V = 200, 220, 240, 260, 280$m/s.

observing Figure 4.7, where d_{min} was obtained as a function of $\bar{w}$. In that figure, one can appreciate that the minimum distance between aircraft decreases as $\bar{w}$ increases in the first scenario, that is to say, the conflict is more severe for higher values of the wind mean; as a consequence of this drop in d_{min}, the probability of being in loss of separation increases. A similar analysis can be done for the second scenario.

In Figure 4.12, the effects of the aircraft airspeeds are represented for $\bar{w} = 0$m/s, $\delta_w = 20$m/s and $V = 200, 220, 240, 260$ and 280m/s. As expected, for higher values of V the certainty of the existence of a conflict decreases: in scenario 1, where the deterministic analysis does not predict a loss of separation, the probability decreases for higher values of V, whereas in scenario 2, where a loss of separation in predicted by the deterministic analysis, the probability increases with V.

4.6 Conflict probability

The conflict probability throughout the trajectory P_{con} is now studied for different values of the wind mean, the aircraft airspeeds and the wind width.

In Figure 4.13, the probability of conflict P_{con} is represented for both scenarios as a function of $\bar{w}$, for $\delta_w = 0, 5, 10, 15, 20$ and 25m/s, where the value $\delta_w = 0$m/s represents the deterministic case (depicted with a thick line). The deterministic analysis predicts a loss of separation for values of the wind mean larger than $\bar{w} = 6.2$m/s in the first scenario and smaller than $\bar{w} = 8.9$m/s in the second one.

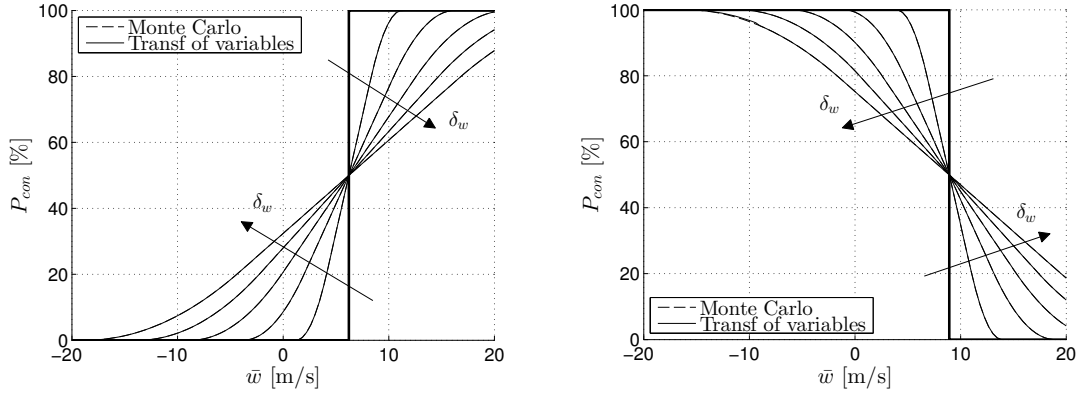

(a) P_{con} for scenario 1.

(b) P_{con} for scenario 2.

Figure 4.13 Probability of conflict P_{con} as a function of $\bar{w}$, for $\delta_w = 0, 5, 10, 15, 20, 25$m/s and $V = 240$m/s.

Regarding the effect of the mean wind, the probability of conflict increases with $\bar{w}$ for all values of δ_w in scenario 1, due to the fact that the minimum distance between aircraft decreases with $\bar{w}$. The opposite behaviour is found in scenario 2.

As in the previous section, the effect of δ_w depends on whether a loss of separation is deterministically predicted or not: for values where the deterministic P_{con} is zero, higher values of δ_w yield an increase in the probability of conflict; on the other hand, for values where a conflict is predicted in the deterministic case, the probability of conflict decreases as δ_w increases.

In Figure 4.14, P_{con} is represented as a function of V for $\delta_w = 0, 10, 15, 20$ and 25m/s.

The obtained results are to be expected: in situations where the conflict is not predicted deterministically, such as in scenario 1, an increment in V (or a decrement in δ_w) translates into smaller values of P_{con}; on the contrary, when a loss of separation exists in the deterministic case, like in scenario 2, the probability of conflict decreases when V increases and δ_w decreases.

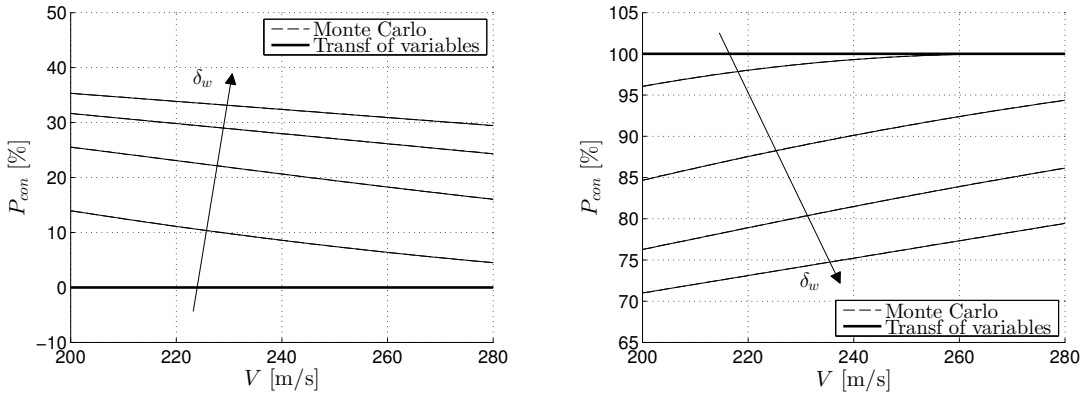

(a) P_{con} for scenario 1.

(b) P_{con} for scenario 2.

Figure 4.14 Probability of conflict P_{con} as a function of V, for $\bar{w} = 0$ and $\delta_w = 0, 5, 10, 15, 20, 25$m/s.

4.7 Duration of the loss of separation

Probability distribution

In this section, the density function of the duration of the loss of separation Δt is obtained. Since this parameter is only defined when there is a loss of separation, the *conditioned probability distribution* of Δt given $P_{con} > 0$ has been computed. The conditioned PDF can be obtained as

$$f_{\Delta t}(\Delta t | P_{con} > 0) = \frac{f_{\Delta t}(\Delta t)}{P_{con}} \tag{4.3}$$

In Figures 4.15 and 4.16, the sought conditioned PDFs and their correspondent S sets have been represented for scenarios 1 and 2, respectively. Additionally, the regions where the indicator is defined in the R sets in the $w_x w_y$ plane have been depicted; in scenario 1 it is defined by the points b,c,d, and e, and in scenario 2 by the points a,b,d,e, and f. The PDFs have been obtained for $\bar{w} = 0$m/s, $\delta_w = 20$m/s and $V = 240$m/s.

The obtained PDFs for this indicator differ quite a bit from $t_{d_{min}}$ and d_{min} ones. For scenario 1, the S set presents again four corners (e, d, c and b), but this time they do not correspond to the cornets in the original R set as in the previous cases. Notice that for values of Δt from points b,e (0s) to point d (26.12s), the limits of integration remain the same (-20m/s to 20m/s); however, the PDF increases almost lineally between these points. This clearly shows how variable the partial derivative $\partial w_x / \partial \Delta t$ is throughout the R set.

In the second scenario, the S set presents five corners (b,d,a,e and f). The relevance of the partial derivative values in the outcome is also obvious in this case: from points b,d (0s) to point a (7.06s), the upper and lower

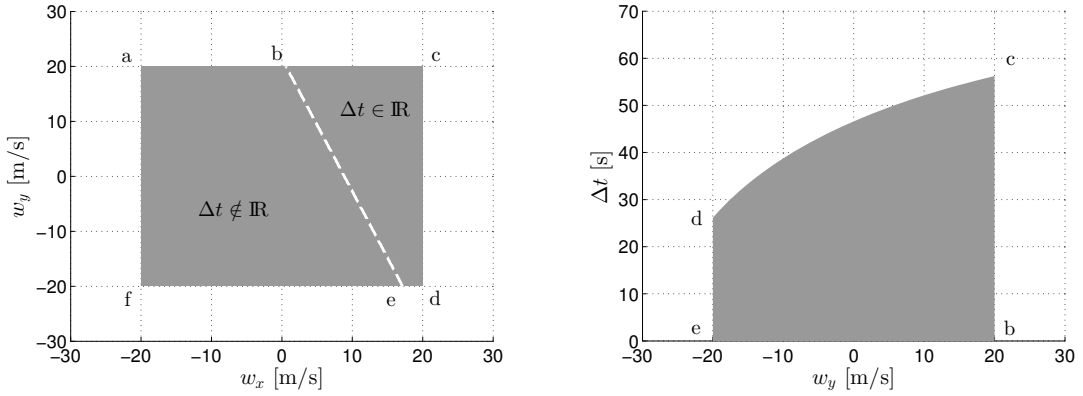

(a) R set in the $w_x w_y$ plane for scenario 1.

(b) S set in the $\Delta t w_y$ plane for scenario 1.

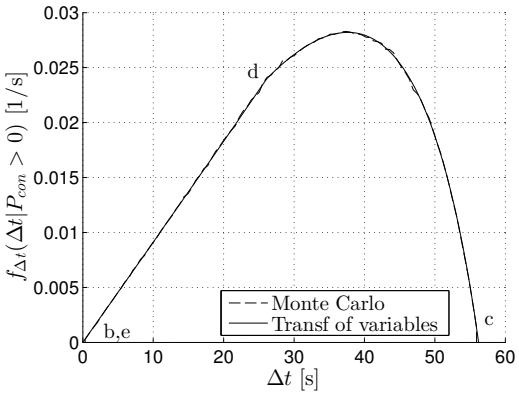

(c) Conditioned PDF for Δt for scenario 1.

Figure 4.15 Wind domain, transformed domain and conditioned probability distribution of Δt, for $\bar{w} = 0$m/s, $\delta_w = 20$m/s and $V = 240$m/s for scenario 1.

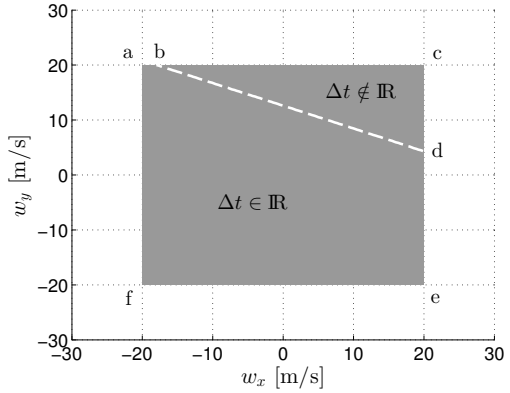

(a) R set in the $w_x w_y$ plane for scenario 2.

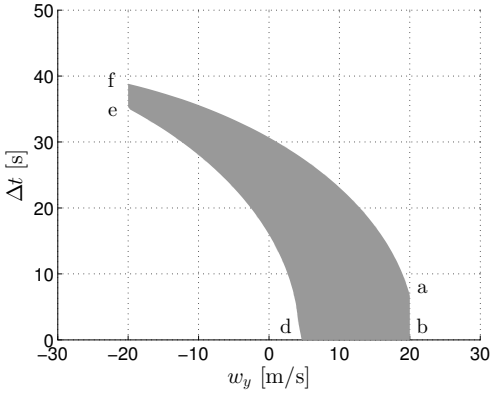

(b) S set in the $\Delta t w_y$ plane for scenario 2.

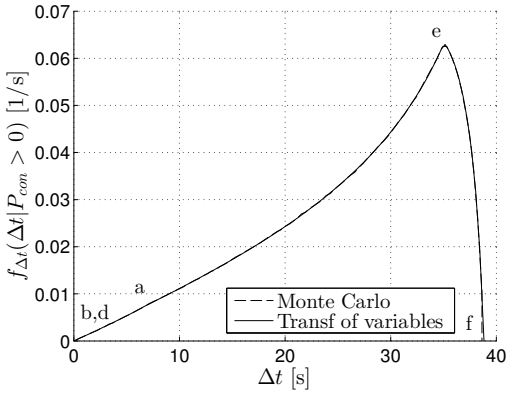

(c) Conditioned PDF for Δt for scenario 2.

Figure 4.16 Wind domain, transformed domain and conditioned probability distribution of Δt, for $\bar{w} = 0$m/s, $\delta_w = 20$m/s and $V = 240$m/s for scenario 2.

limits of integration remain almost constant, but the PDF increases between these points; from a to e (35.3s), the value of the PDF significantly increases despite being the limits of integration closer to each other.

The relatively odd shapes of the S sets for this indicator and the changing values of $\partial w_x / \partial \Delta t$ may be due to the fact that this indicator is defined by quite a complex equation (see eq. [2.12] in Chapter 2) in comparison to $t_{d_{min}}$ and d_{min} indicators.

In Table 4.4, the correspondent values of the mean and standard deviation of Δt are collected for transformation of variables and Monte Carlo methods.

Table 4.4 Expected value and standard deviation of Δt, conditioned to the existence of a conflict.

	Scenario 1		Scenario2	
Method	$E[\Delta t]$	$\sigma[\Delta t]$	$E[\Delta t]$	$\sigma[\Delta t]$
Transformation of variables	32.40s	12.39s	26.55s	8.65s
Monte Carlo	32.40s	12.39s	26.57s	8.65s

Effect of the wind uncertainty

Next, the influence of the wind parameters $\bar{w}$ and δ_w on Δt is analysed. In Figure 4.17, $E[\Delta t]$ and $\sigma[\Delta t]$ are represented as a function of $\bar{w}$ for $\delta_w = 5, 10, 15, 20$ and 25m/s and $V = 240$m/s. The results shown in this section are not conditioned to the existence of a conflict; when $P_{con} = 0$, the indicator Δt has been set to zero.

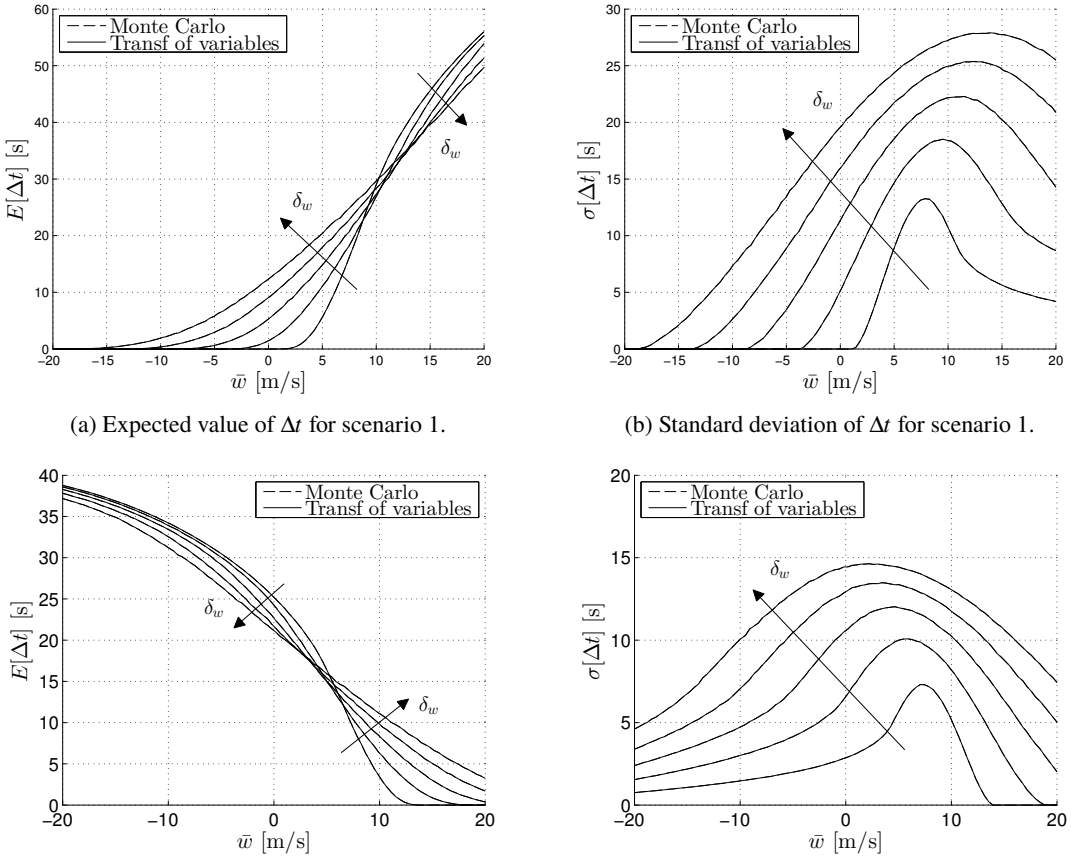

(a) Expected value of Δt for scenario 1.

(b) Standard deviation of Δt for scenario 1.

(c) Expected value of Δt for scenario 2.

(d) Standard deviation of Δt for scenario 2.

Figure 4.17 Expected value and standard deviation of Δt as a function of $\bar{w}$, for $\delta_w = 5, 10, 15, 20, 25$m/s and $V = 240$m/s.

If one compares these graphics with the ones in Figure 4.13, it is clear that indicators Δt and P_{con} are strictly related: higher values of P_{con} translate into a more severe conflict situation, and thus, to higher expected values of the duration of the loss of separation.

As seen in section 4.6, the probability of conflict increases when $\bar{w}$ increases in scenario 1 (while decreases in scenario 2), and so does the expected value of the duration of the conflict. Regarding the standard deviation,

Figure 4.17 shows that higher levels of dispersion are obtained for wind mean values around $\bar{w} = 6.2$m/s in scenario 1 and $\bar{w} = 8.9$m/s in scenario 2, which correspond with the wind mean values that limits the existence of a conflict for the deterministic case.

Unlike other indicators, the variable δ_w now affects the expected value of Δt: for $\bar{w}$ values where the conflict is detected in the deterministic analysis, increments of δ_w yield to higher values of $E[\Delta t]$, while the opposite is true when no conflict exists in the deterministic case.

For $\sigma[\Delta t]$, the behaviour is now similar to other indicators: the standard deviation of Δt increases for higher values of δ_w.

Effect of the aircraft airspeeds

Finally, the effect of the aircraft airspeeds V on $E[\Delta t]$ and $\sigma[\Delta t]$ is studied in this section. Figure 4.9 depicts the expected value and standard deviation of Δt as a function of V for $\bar{w} = 0$m/s and $\delta_w = 5, 10, 15, 20$ and 25m/s.

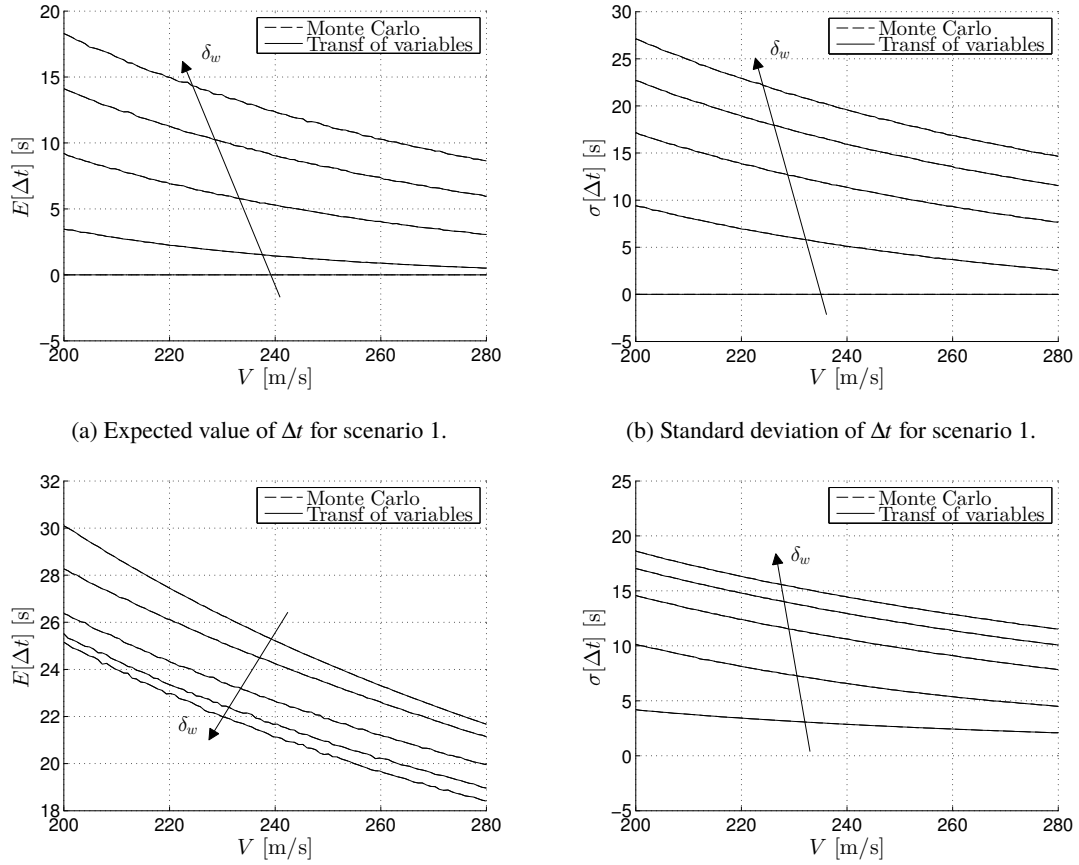

(a) Expected value of Δt for scenario 1.

(b) Standard deviation of Δt for scenario 1.

(c) Expected value of Δt for scenario 2.

(d) Standard deviation of Δt for scenario 2.

Figure 4.18 Expected value and standard deviation of Δt as a function of V, for $\bar{w} = 0$m/s and $\delta_w = 5, 10, 15, 20, 25$m/s.

As the figure shows, expected value of Δt decreases when the aircraft airspeeds increases, which is a perfectly predictable result, given the fact that faster aircraft will exit the loss of separation sooner than slower ones.

The evolution of $\sigma[\Delta]$ with V is very similar to $t_{d_{min}}$ and d_{min} cases: when V increases, the standard deviation decreases, a tendency that is more important for higher values of δ_w.

5 Conclusions and future work

In this project, the transformation of random variables method has been successfully applied to the probabilistic study of aircraft conflict detection in presence of uncertain wind. The results have been validated using the Monte Carlo method. Both methods yield practically identical results.

Conflict indicators like the time to minimum distance, minimum distance or the duration of the loss of separation have been defined to characterize the intensity of the conflict situation. In particular, the probability of the existence of a conflict is a parameter of great interest in the present analysis. The influence of the wind uncertainty and aircraft airspeeds on these indicators has been studied for two different scenarios. The evolution of the indicators has been found to be different for each scenario, proving that this evolution depends on the relative position and movement between the aircraft.

The application of the transformation of random variables methodology has proven to be very useful to analyse the probability density functions of the indicators, and thus, their statistic characteristics expected value and standard deviation. In particular, the study of the transformed domains obtained with this method has helped to fully understand the behaviour of the indicators' distributions.

A uniform wind distribution has been considered. However, the methodology herein described is applicable to any wind distribution.

Among the most interesting results obtained throughout this work are the following:

- The expected value of the indicators differs from the one obtained in a deterministic analysis for the average wind, which is due to the non-linear dependence of the indicators on the wind parameters;
- higher values of the aircraft airspeeds contribute to the reduction of uncertainty; and
- the certainty that a conflict exists or does not exist decreases when the wind dispersion increases or the aircraft airspeeds decrease.

This project constitutes a first step in the development of a methodology to manage weather uncertainty in the context of conflict detection and resolution. The safety and efficiency of the air traffic management are expected to be beneficed from the inclusion of weather uncertainty in automated conflict detection by allowing the trajectories to be strategically deconflicted in the long range planning and reducing the number of missed and false alerts in the mid and short terms.

Next steps in the present line of investigation would include:

- The application of the methodology to other conflict indicators, such as the instant of time when a loss of separation is detected or the position of each aircraft along its trajectory where the LOS takes place.
- Probabilistic analysis considering different types of wind distributions. Among the possible distributions, the use of a wind PDF obtained from an actual ensemble weather forecast would be of great interest.
- The use of the methodology on more complex scenarios, such as trajectories composed on several cruise segments with different courses or the presence of more than two aircraft in the same airspace.
- The consideration of correlated wind-fields in which the wind velocity varies with the position.

List of Figures

List of Tables

Bibliography

[1] *IMET - Investigating the optimal approach for future trajectory prediction (TP) systems to use METeorological uncertainty information. SESAR WP-E Project 02.40*, http://sesarinnovationdays.eu/files/2013/Posters/SID%202013%20poster%20IMET.pdf, 2013, Poster in 3rd SESAR Innovation Days (SID2013).

[2] C Bayer, H Hoel, E Von Schwerin, and R Tempone, *On NonAsymptotic Optimal Stopping Criteria in Monte Carlo Simulations*, SIAM Journal on Scientific Computing **36** (2014), no. 2, A869–A885.

[3] J Cheung, JL Brenguier, A Hally, J Heijstek, and A Marsman, *Recommendations on Trajectory Selection in Flight Planning based on Weather Uncertainty*, 5th SESAR Innovation Days, Bologna, Italy (2015).

[4] E Gutiérrez Moya and M Gutiérrez Fernández, *Estadística en la ingeniería. Probabilidad*, Digital @tres, Sevilla, 2004.

[5] RV Hogg and Craig AT, *Introduction to Mathematical Statistics*, Prentice-Hall International, Englewood Cliffs, NJ, 1995.

[6] B Lapeyre, *Introduction to Monte-Carlo Methods*, Lecture, Halmstad, Sweden (2007), 2–4.

[7] ComplexWorld Research Network, *Complexity concepts in ATM*, http://complexworld.eu/wiki/Complexity_concepts_in_ATM, 2016, from ComplexWorld Network's wiki.

[8] ———, *Uncertainty in ATM*, http://complexworld.eu/wiki/Uncertainty_in_ATM, 2016, from ComplexWorld Network's wiki.

[9] T Perlinger, *Probability Theory: Multivariate random variables*, University Lecture, Uppsala University, 2012.

[10] WH Press, SA Teukolsky, WT Vetterling, and BP Flannery, *Numerical Recipes in Fortran 77. The Art of Scientific Computing*, Fortran Numerical Recipes, vol. 1, Press Syndicate of the University of Cambridge, New York, 2 ed., 1997, pp. 180–184.

[11] JM Sloughter, T Gneiting, and AE Raftery, *Probabilistic Wind Speed Forecasting using Ensembles and Bayesian Model Averaging*, Journal of the American Statistical Association **105** (2010), no. 489, 25–35.

[12] M Steiner, *Translation of Ensemble-based Weather Forecasts into Frobabilistic Air Traffic Capacity Impact*, 2009 IEEE/AIAA 28th Digital Avionics Systems Conference, IEEE, 2009, pp. 2–D.

[13] R Vázquez and D Rivas, *Analysis of the Effect of Uncertain Average Winds on Cruise Fuel Load*, 5th SESAR Innovation Days, Bologna, Italy (2015).

[14] AL Visintini, W Glover, J Lygeros, and J Maciejowski, *Monte Carlo Optimization for Conflict Resolution in Air Traffic Control*, IEEE Transactions on Intelligent Transportation Systems **7** (2006), no. 4, 470–482.

[15] EW Weisstein, *Monte Carlo Method*, http://mathworld.wolfram.com/MonteCarloMethod.html, From *MathWorld.com*, a Wolfram Web Resource.

[16] JW Wittwer, *Monte Carlo Simulation Basics*, http://www.vertex42.com/ExcelArticles/mc/MonteCarloSimulation.html, June 2004, From Vertex42.com.

Detección Probabilística de Conflictos entre Aeronaves utilizando Transformación de Variables Aleatorias

Trabajo de Fin de Máster. Resumen

Autor: Eulalia Hernández Romero Tutor: Alfonso Valenzuela Romero

1. Introducción

Motivación

El sistema de gestión del tráfico aéreo (ATM) es un sistema complejo con un gran número de agentes que interactúan entre ellos. Como cualquier sistema complejo, el sistema ATM presenta incertidumbre, que puede ser debida a factores humanos, dinámicas desconocidas o errores en las medidas. En concreto, la incertidumbre introducida por el carácter impredecible de la atmósfera (aparición de nieblas, velocidad del viento, tormentas...) es especialmente importante y es causante de un gran número de retrasos y cancelaciones.

El estudio y gestión de la incertidumbre meteorológica puede beneficiar en gran medida a la gestión del tráfico aéreo, mejorando su eficiencia y seguridad.

Una de las líneas de investigación actualmente más populares para la inclusión del estudio de la incertidumbre meteorológica en la predicción de trayectorias de aeronaves es el uso de Sistemas de Predicción por Conjuntos. Estos sistemas se basan en evaluar repetidamente un modelo de predicción para variaciones pequeñas de las condiciones iniciales y/o diferentes parametrizaciones físicas, para obtener un conjunto de predicciones, compuestos por un número de predicciones (o miembros) de entre 10 y 50. El proyecto IMET [1] [3] describe dos enfoques diferentes en cuanto a la predicción probabilistica de trayectorias usando predicción meteorológica por ensambles:

1. **Predicción probabilística de trayectorias:** Los parámetros de interés de la trayectoria se derivan directamente de la distribuciones de probabilidad de las variables meteorológicas, utilizando un predictor de trayectorias probabilístico.
2. **Predicción de trayectorias por conjuntos:** En este enfoque, se aplica un predictor de trayectorias determinista a cada miembro del conjunto, obteniendo un conjunto de trayectorias.

El proyecto IMET seguía este segundo enfoque. En este trabajo se va a seguir el primero.

Objetivos

El objetivo del trabajo es estudiar la situación de conflicto en la que dos aeronaves se aproximan con velocidad, rumbo y altitud constantes en el mismo nivel de vuelo y bajo la presencia

de vientos desconocidos, definidos por su función de densidad. Se considera que un conflicto se produce cuando se predice que en el futuro las aeronaves se encontrarán en pérdida de separación, es decir, cuando se predice que las aeronaves se encontrarán a una distancia entre ellas menor que un margen mínimo de separación. El conflicto se va caracterizar por una serie de indicadores, tales como la mínima distancia entre aeronaves, el instante de tiempo en el que se alcanza esta distancia o la probabilidad de que se produzca el conflicto.

Se va a realizar un estudio probabilístico usando transformación de variables aleatorias. Los resultados obtenidos serán comparados y validados usando el método de Monte Carlo.

Para dos escenarios diferentes, se van a estudiar los efectos de las propiedades estadísticas del viento, tales como su media o varianza, y de la velocidad de las aeronaves sobre los indicadores.

2. Planteamiento del problema

Escenario

El escenario general considerado en este proyecto es el que se muestra en la Figura 1.

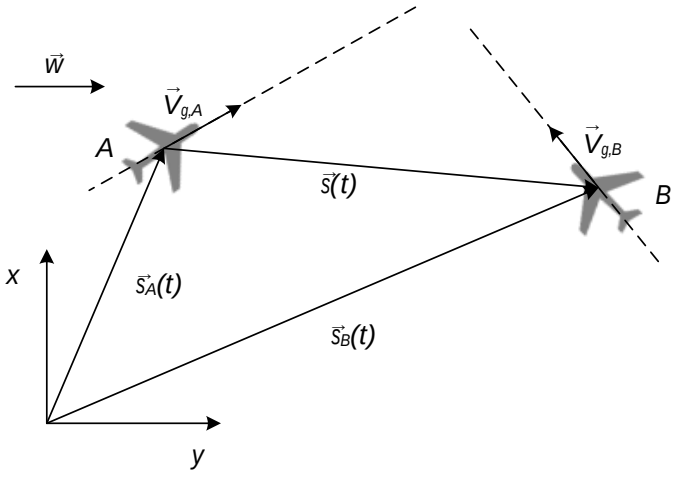

Figura 1: Escenario general

Este escenario viene definido por los siguientes supuestos:

- las dos aeronaves vuelan en el mismo espacio aéreo y nivel de vuelo;
- las derrotas y velocidades aerodinámicas de las aeronaves son constantes y conocidas, así como sus posiciones iniciales;
- las aeronaves se encuentran suficientemente cerca como para suponer que están expuestas al mismo viento;
- el viento es incierto; y

- la distancia entre aeronaves en el instante inicial es mayor que un margen mínimo de separación D.

En este escenario, la posición de las aeronaves A y B puede escribirse como

$$\begin{aligned}\vec{s}_A(t) &= \vec{s}_{A0} + \vec{V}_{gA}t = \vec{s}_{A0} + (\vec{V}_A(t) + \vec{w})t \\ \vec{s}_B(t) &= \vec{s}_{B0} + \vec{V}_{gB}t = \vec{s}_{B0} + (\vec{V}_B(t) + \vec{w})t\end{aligned} \tag{1}$$

siendo $\vec{V}_{g,i}$ la velocidad con respecto a tierra, $\vec{V}_i$ la velocidad aerodinámica y $\vec{s}_{0,i}$ la posición inicial de cada aeronave.

La distancia entre aeronaves viene dada por

$$d(t) = \sqrt{s_0^2 + 2\vec{s}_0\vec{V}_g t + V_g^2 t^2} \tag{2}$$

donde $\vec{s}_0 = \vec{s}_{0,B} - \vec{s}_{0,A}$ es la posición inicial relativa entre aeronaves y $\vec{V}_g = \vec{V}_{g,B} - \vec{V}_{g,B}$ es la velocidad relativa con respecto a tierra.

Indicadores

Los indicadores que se han escogido para caracterizar el conflicto son los siguientes.

- *Tiempo para la distancia mínima*

$$\frac{d(d(t))}{dt} = \frac{1}{2}\frac{2\vec{s}_0.\vec{V}_g + 2V_g^2 t}{d(t)} = 0 \rightarrow t_{d_{min}} = \frac{-\vec{s}_0.\vec{V}_g}{V_g^2} \tag{3}$$

- *Distancia mínima*

$$d_{min} = \sqrt{s_0^2 - 2\vec{s}_0\vec{V}_g\frac{\vec{s}_0.\vec{V}_g}{V_g^2} + V_g^2\frac{(\vec{s}_0.\vec{V}_g)^2}{V_g^4}} = \sqrt{s_0^2 - \frac{(\vec{s}_0.\vec{V}_g)^2}{V_g^2}} \tag{4}$$

- *Probabilidad de pérdida de separación en un instante de tiempo t*

$$P[d(t) \leq D] \tag{5}$$

- *Probabilidad de conflicto*

$$P[d_{min} \leq D] \tag{6}$$

- *Duración de la pérdida de separación*

$$\Delta t = 2\sqrt{\frac{(\vec{s}_0.\vec{V}_g)^2}{V_g^4} - \frac{(s_0^2 - D^2)}{V_g^2}} = 2\sqrt{t_{dmin}^2 - \frac{(s_0^2 - D^2)}{V_g^2}} \tag{7}$$

Incertidumbre en la velocidad

Los indicadores anteriores dependen de la velocidad $\vec{V}_g$. Dado que ésta depende del viento, es necesario obtener su expresión con respecto a las componentes de la velocidad del viento. En este proyecto el viento va a quedar definido por su componente norte w_x y su componente este w_y. La velocidad relativa con respecto a tierra viene dada por la siguiente expresión:

$$\vec{V}_g = \vec{V}_B - \vec{V}_A = V_B \begin{bmatrix} cos\big(\psi_B - arcsin\big(\frac{w_{c,B}}{V_B}\big)\big) \\ sin\big(\psi_B - arcsin\big(\frac{w_{c,B}}{V_B}\big)\big) \end{bmatrix} - V_A \begin{bmatrix} cos\big(\psi_A - arcsin\big(\frac{w_{c,A}}{V_A}\big)\big) \\ sin\big(\psi_A - arcsin\big(\frac{w_{c,A}}{V_A}\big)\big) \end{bmatrix} \tag{8}$$

donde los términos $w_{c,i}$ hacen referencia al viento cruzado, que puede expresarse como

$$w_{c,A} = w_y cos\psi_A - w_x sin\psi_A \tag{9}$$

$$w_{c,B} = w_y cos\psi_B - w_x sin\psi_B \tag{10}$$

Como puede verse, $\vec{V}_g$ sólo depende del viento cruzado, mientras que $\vec{V}_{g,A}$ y $\vec{V}_{g,B}$ también dependen del viento paralelo a la dirección de la trayectoria de cada aeronave.

Modelo probabilístico de viento

En este proyecto se va a considerar unos vientos distribuidos uniformemente, con la siguiente función de densidad para sus componentes w_x y w_y:

$$f_{w_i}(w_i) = \begin{cases} \frac{1}{2\delta_{w_i}}, & w_i \in [\bar{w}_i - \delta_{w_i}, \bar{w}_i + \delta_{w_i}] \\ 0 & \text{en otros casos} \end{cases} \tag{11}$$

donde $2\delta_{w,i}$ es el ancho de la función de densidad. Dado que ambas componentes son independientes, la función de densidad conjunta puede expresarse como

$$f_{w_x,w_y}(w_x, w_y) = f_{w_x}(w_x) \cdot f_{w_y}(w_y) = \frac{1}{4}\frac{1}{\delta w_x \delta w_y}, \qquad w_i \in [\bar{w}_i - \delta w_i, \bar{w}_i + \delta w_i] \tag{12}$$

3. Transformación de variables aleatorias

Para obtener las funciones de densidad de probabidad (f.d.d o PDF) de los indicadores a estudiar se ha utilizado el método de transformación de variables aplicado al caso de dos variables aleatorias. Este método consiste en obtener la función de densidad de la variable de interés a partir de la función de densidad de las variables de las que ésta depende.

Considérese dos variables aleatorias u_1 y u_2 con función de densidad conjunta f_{u_1,u_2} conocida con dominio R. Sea v_1 y v_2 dos variables aleatorias tal que

$$\begin{aligned} v_1 &= g_1(u_1, u_2) \\ v_2 &= g_2(u_1, u_2) \end{aligned} \tag{13}$$

con una función de densidad $f_{v_1,v_2}(v_1, v_2)$ que se desea obtener. Si la transformación $g_1(u_1, u_2)$ y $g_2(u_1, u_2)$ es bijectiva y transforma el recinto R del plano u_1u_2 en el recinto S del plano v_1v_2,

la función de densidad buscada puede calcularse como

$$f_{v_1,v_2}(v_1,v_2) = f_{u_1,u_2}(h_1(v_1,v_2),h_2(v_1,v_2)) \cdot |J(v_1,v_2)| \tag{14}$$

donde la inversa de la transformación viene dada por $u_1 = h_1(v_1,v_2)$ y $u_2 = h_2(v_1,v_2)$, y J es el Jacobiano de la transformación.

$$J = \begin{vmatrix} \frac{\partial u_1}{\partial v_1} & \frac{\partial u_1}{\partial v_2} \\ \frac{\partial u_2}{\partial v_1} & \frac{\partial u_2}{\partial v_2} \end{vmatrix} = \begin{vmatrix} \frac{\partial h_1(v_1,v_2)}{\partial v_1} & \frac{\partial h_1(v_1,v_2)}{\partial v_2} \\ \frac{\partial h_2(v_1,v_2)}{\partial v_1} & \frac{\partial h_2(v_1,v_2)}{\partial v_2} \end{vmatrix} \tag{15}$$

La función de densidad marginal $f_{v_1}(v_1)$ se puede calcular de la siguiente forma

$$f_{v_1}(v_1) = \int_{-\infty}^{\infty} f_{v_1,v_2}(v_1,v_2)dv_2 \tag{16}$$

En el problema que se estudia en este proyecto, las velocidades w_x y w_y toman el lugar de u_1 y u_2. La variable v_1 es el indicador a estudiar y v_2 se considera una variable auxiliar, que por simplicidad se ha tomado igual a w_y. El método de transformación de variables particularizado al presente problema quedaría como

$$f_{v_1}(v_1) = \int_{w_y} f_{v_1,w_y}(v_1,w_y)dw_y = \frac{1}{4}\frac{1}{\delta w_x \delta w_y}\int_{w_y} \left|\frac{\partial w_x(v_1,w_y)}{\partial v_1}\right| dw_y \tag{17}$$

En el caso de que la transformación fuera no monótona en el dominio R, sería necesario dividir el dominio en regiones R_j donde la transformación fuese monótona, calcular la función de densidad marginal en estas regiones y finalmente sumarlas.

Dado que las ecuaciones que definen los indicadores no permiten obtener expresiones analíticas de las derivadas parciales ni de las transformaciones inversas, éstas se han calculado numéricamente usando la herramienta de software matemático MATLAB.

4. Método de Monte Carlo

El método de Monte Carlo se ha usado en este proyecto para validar los resultados obtenidos con el método de transformación de variables.

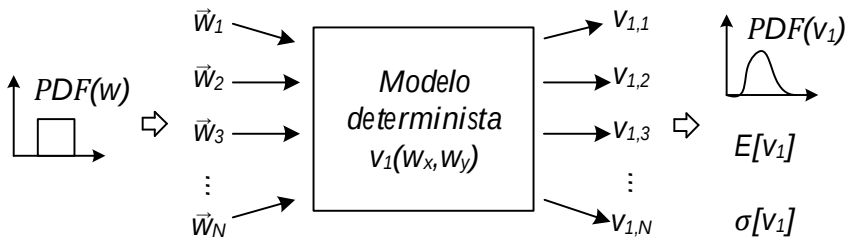

Figura 2: Método de Monte Carlo

Este método, basado en la ley de los grandes números, consiste en evaluar repetidamente un modelo determinista usando una muestra aleatoria como entrada, para obtener otra muestra

aleatoria a la salida de la cual obtener información estadística, como la media, varianza o la función de distribución de la variable de interés.

El método de Monte Carlo se ha aplicado a este problema considerando muestras aleatorias de las componentes del viento $\{w_{x,k}, w_{y,k}\}$. Estas muestras se usan para evaluar las funciones de los indicadores y así obtener una muestra de la solución $\{v_{1,k}\}$ de la cual se obtiene información estadística.

El número de muestras utilizado en las simulaciones de Monte Carlo llevadas a cabo en este proyecto ha sido $N = 2^{23} = 8{,}4 \cdot 10^6$

5. Resultados

Se han obtenido resultados para el caso en el que las dos componentes del viento siguen funciones de distribución idénticas $\bar{w}_x = \bar{w}_y = \bar{w}$ y $\delta_{w_x} = \delta_{w_y} = \delta_w$. Las velocidades aerodinámicas de las aeronaves también se han considerado iguales $V_A = V_B = V$. Los resultados mostrados en este documento se han obtenido para $\bar{w} = 0$m/s, $\delta_w = 20$m/s y $V = 240$m/s.

Escenarios

Los resultados se han obtenido para dos escenarios diferentes:

- **Escenario 1:** $\vec{s}_{0,A} = [0, 0]$, $\vec{s}_{0,B} = [10, 10]$NM$= [18520, 18520]$m, $\psi_A = 90°$ y $\psi_B = 135°$
- **Escenario 2:** $\vec{s}_{0,A} = [0, 0]$, $\vec{s}_{0,B} = [25, 50]$NM$= [46300, 92600]$m, $\psi_A = 90°$ y $\psi_B = 225°$

Tiempo para la distancia mínima

La función de densidad para el indicador $t_{d_{min}}$ en cada escenario se muestra en la Figura 4. Puede verse como el recinto transformado presenta 4 esquinas (a, b c y d en la figura) y cómo estas esquinas se traducen en cambios bruscos en la función de densidad.

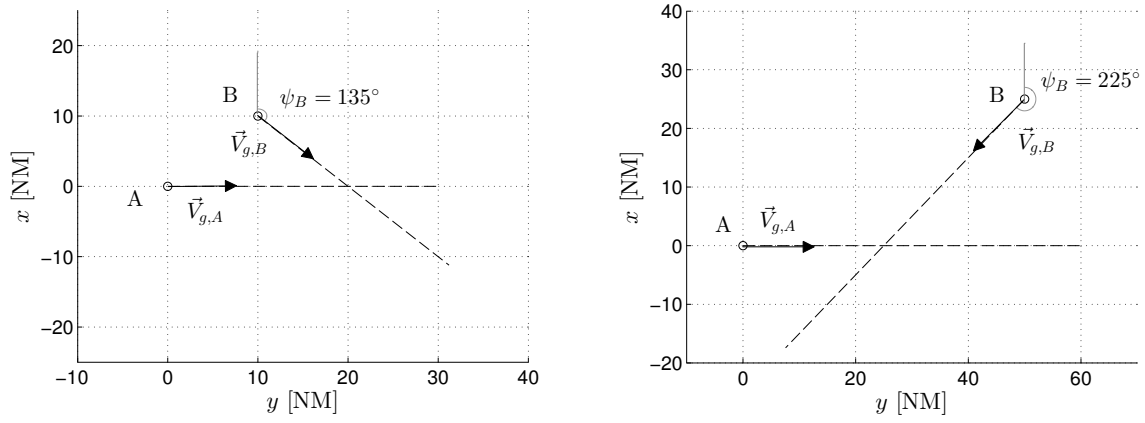

(a) Escenario 1

(b) Escenario 2

Figura 3: Escenarios

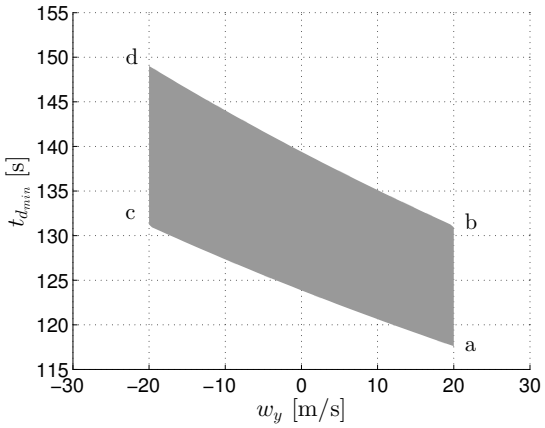

(a) Región S en el plano $t_{d_{min}} w_y$ para el escenario 1

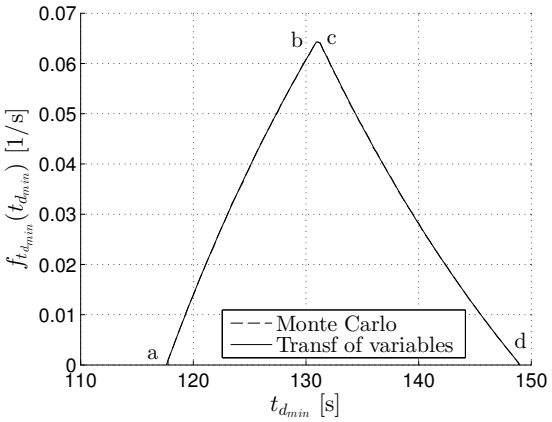

(b) PDF de $t_{d_{min}}$ para el escenario 1

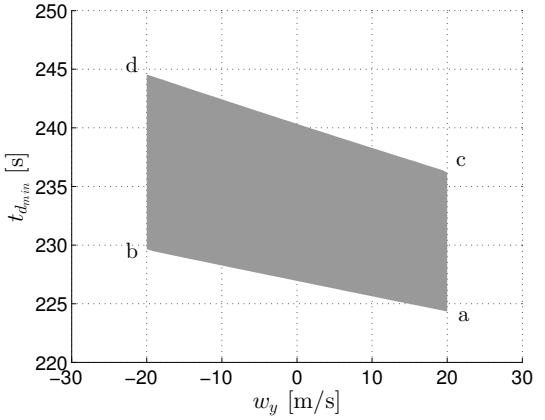

(c) Región S en el plano $t_{d_{min}} w_y$ para el escenario 2

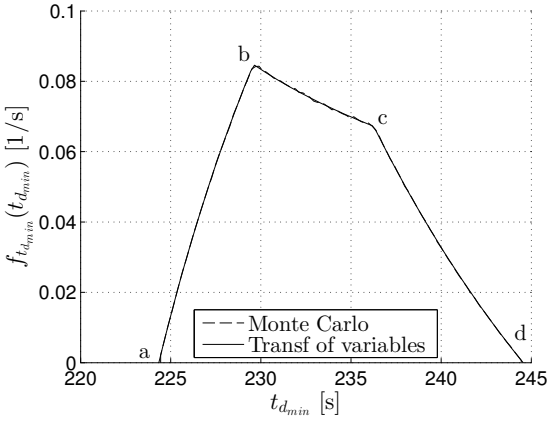

(d) PDF de $t_{d_{min}}$ para el escenario 2

Figura 4: Dominio S y función de densidad de $t_{d_{min}}$ para $\bar{w} = 0$m/s, $\delta_w = 20$m/s y $V = 240$m/s.

Se ha encontrado que la media del indicador $E[t_{d_{min}}]$ es prácticamente constante con $\bar{w}$ y δ_w, mientras que disminuye con V. La desviación estándar $\sigma[t_{d_{min}}]$ aumenta al aumentar δ_w y disminuye al aumentar V, mientras que su evolución varía según el escenario que consideremos (disminuye con $\bar{w}$ en el escenario 1 y aumenta en el escenario 2).

Distancia mínima entre aeronaves

En la Figura 5 se muestran los recintos transformados y las funciones de densidad de la variable d_{min} para ambos escenarios. La línea vertical D muestra el mínimo de separación fijado (5NM).

De nuevo, los recintos muestran 4 esquinas que constituyen cambios bruscos de pendiente en la PDF. En el caso de d_{min}, puede verse que los puntos a,b,c y d están unidos prácticamente por líneas rectas, lo que indica que el jacobiano de la transformación es constante en todo el dominio.

El valor medio de la distancia mínima disminuye con $\bar{w}$ en el escenario 1 y aumenta en el escenario 2. Se ha encontrado que $E[d_{min}]$ no depende de δ_w ni de V. La desviación estándar $\sigma[d_{min}]$ aumenta con δ_w y disminuye con V, mientras que variaciones en $\bar{w}$ apenas influyen en este parámetro.

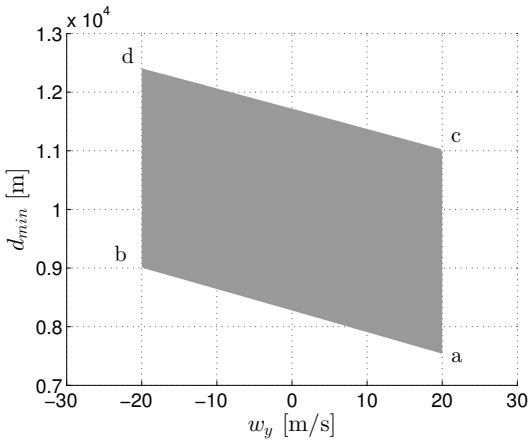

(a) Región S en el plano $d_{min}w_y$ para el escenario 1

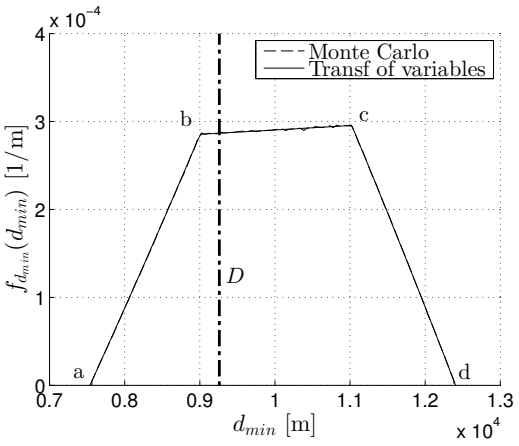

(b) PDF de d_{min} para el escenario 1

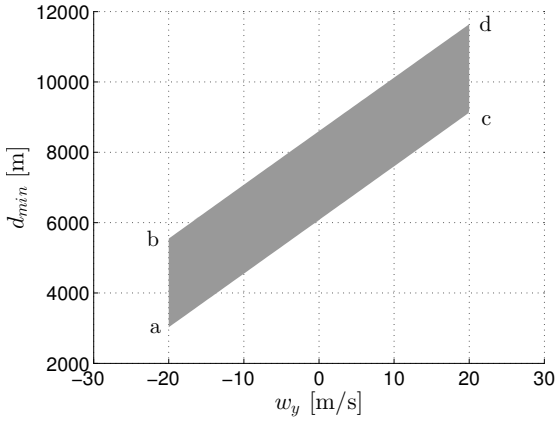

(c) Región S en el plano $d_{min}w_y$ para el escenario 2

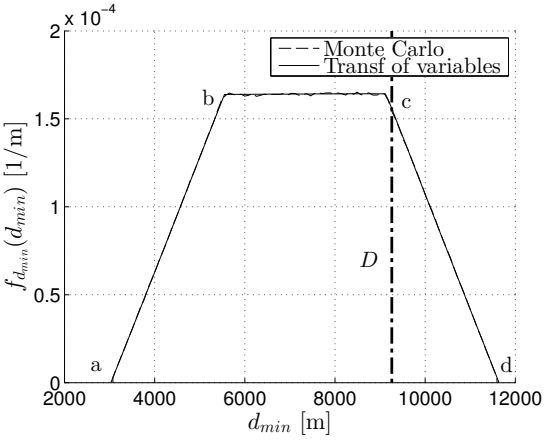

(d) PDF de d_{min} para el escenario 2

Figura 5: Dominio S y función de densidad de d_{min}, para $\bar{w} = 0$m/s, $\delta_w = 20$m/s y $V = 240$m/s

Como excepción, para valores cercanos a $\bar{w} = -20$m/s en el escenario 2 aparece una transformación no monótona donde hay que separar el recinto R en dos, R_1 y R_2. Esto causa una ligera caida en la desviación estándar de d_{min} al aparecer distribuciones menos dispersas.

Probabilidad de pérdida de separación

En este apartado se muestra la probabilidad de la aeronave A de estar en pérdida de separación a lo largo de su trayectoria, lo que puede expresarse como $P[d(r_A/V_{g,A} \leq 5NM)]$. En la Figura 6 se muestra como varía esta probabilidad a lo largo de la trayectoria de A para diferentes valores de δ_w. En una linea más gruesa se muestran los resultados del caso determinista.

La probabilidad es cero al comienzo de la trayectoria, aumenta desde cierto punto y alcanza un máximo para después disminuir hasta cero al alejarse las aeronaves entre sí. Puede verse que cuando el caso determinista no predice una pérdida de separación, aumentos de δ_w producen aumentos de probabilidad, mientras que cuando sí se predice una pérdida de separación, al aumentar δ_w esta probabilidad disminuye.

Adicionalmente, se ha comprobado que $P[d(r_A/V_{g,A} \leq 5NM)]$ aumenta con $\bar{w}$ en el escenario 1 mientras que disminuye en el escenario 2. Valores altos de la velocidad V provocan bajadas de la probabilidad cuando no se predice pérdida de separación y subidas cuando sí se

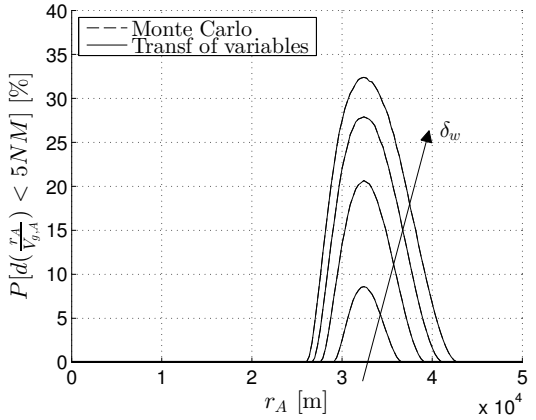

(a) $P[d(r_A/V_{g,A} \leq 5NM)]$ para el escenario 1

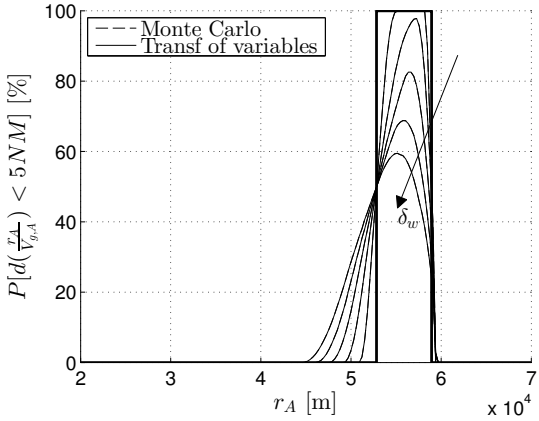

(b) $P[d(r_A/V_{g,A} \leq 5M)]$ para el escenario 2

Figura 6: Probabilidad de que la aeronave A se encuentre en pérdida de separación $P[d(r_A/V_{g,A} \leq 5NM)]$ como función de r_A, para $\bar{w} = 0$, $\delta_w = 0, 5, 10, 15, 20, 25$m/s y $V = 240$m/s

predice en el caso determinista.

Probabilidad de conflicto

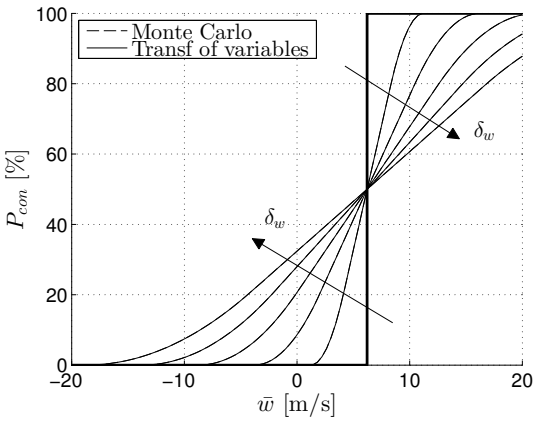

(a) P_{con} para el escenario 1

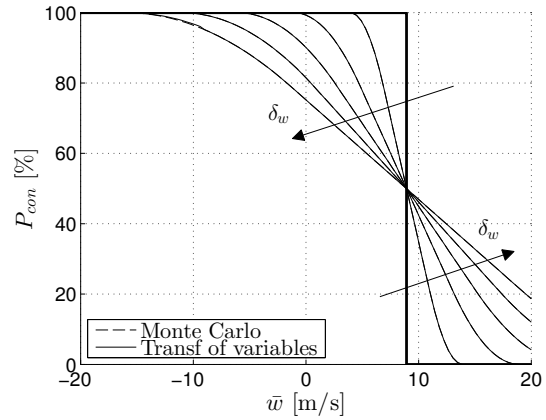

(b) P_{con} para el escenario 2

Figura 7: Probabilidad de conflicto P_{con} como función de $\bar{w}$, para $\delta_w = 0, 5, 10, 15, 20, 25$m/s y $V = 240$m/s

La probabilidad de conflicto se puede obtener a partir de la PDF de d_{min} obteniendo el área bajo la función a la izquierda de la separación mínima D:

$$P_{con} = \int_{-\infty}^{D} f_{d_{min}}(\rho) d\rho \tag{18}$$

En la Figura 7 se muestra cómo varía esta probabilidad como función de la media del viento $\bar{w}$ para diferentes valores de δ_w en los dos escenarios. En una línea más gruesa se muestra de nuevo el caso determinista.

La probabilidad de conflicto aumenta con $\bar{w}$ desde 0 hasta 100 % en el escenario 1, mientras que disminuye en el escenario 2. La influencia de δ_w depende de si se predice o no conflicto

en el caso determinista: por ejemplo, en el escenario 1, para valores de $\bar{w}$ menores a 6.2m/s, la probabilidad aumenta al aumentar δ_w, mientras que para valores mayores disminuye cuando δ_w aumenta.

La influencia de V en P_{con} también depende de si se predice o no conflicto: para casos en los que no se predice conflicto P_{con} disminuye al aumentar V y para casos en los que sí se predice P_{con} aumenta con V.

Duración de la pérdida de separación

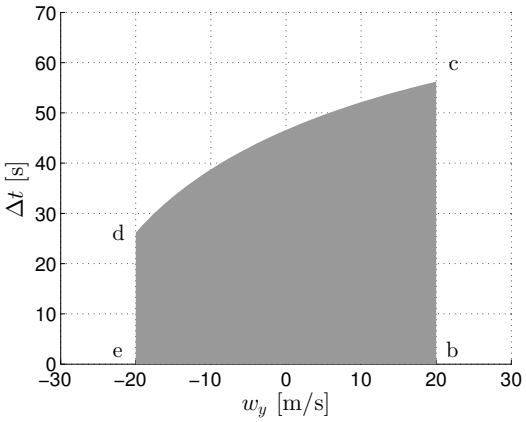

(a) Región S en el plano $\Delta t w_y$ para el escenario 1

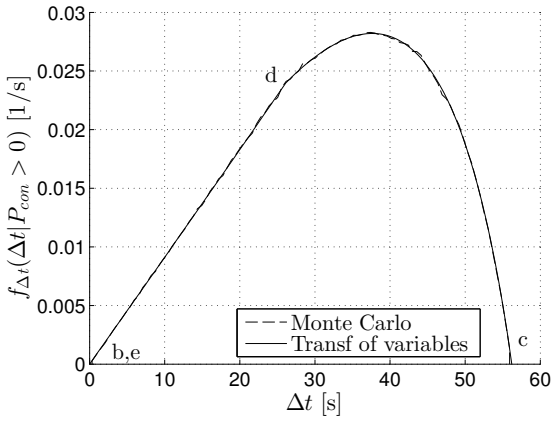

(b) PDF condicionada de Δt para el escenario 1

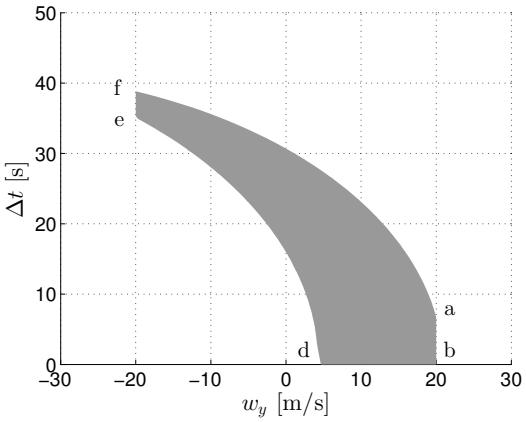

(c) Región S en el plano $\Delta t w_y$ para el escenario 2

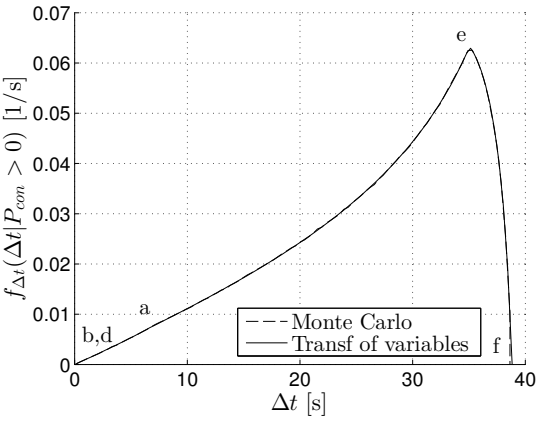

(d) PDF condicionada de Δt para el escenario 2

Figura 8: Dominio S y función de densidad condicionada de Δt, para $\bar{w} = 0$m/s, $\delta_w = 20$m/s y $V = 240$m/s

En este apartado se recogen los resultados relativos al indicador Δt. Dado que este parámetro sólo está definido cuando existe un conflicto se ha obtenido la función de densidad de Δt condicionada a que $P_{con} > 0$. La PDF condicionada se puede calcular como

$$f_{\Delta t}(\Delta t|P_{con} > 0) = \frac{f_{\Delta t}(\Delta t)}{P_{con}} \tag{19}$$

En la Figura 8 se representan los dominios transformados y las funciones de densidad de Δt para los dos escenarios.

De nuevo, los recintos presentan una serie de esquinas que causan cambios en la pendiente de la PDF. Puede verse cómo los límites de integración no tienen tanta relevancia en la forma de la PDF como la tenían en los indicadores anteriores: el valor del Jacobiando de esta transformación es variable a lo largo de todo el dominio.

En cuanto a la media $E[\Delta t]$, se ha comprobado que depende de los factores $\bar{w}$, δ_w y V tal y como lo hace el parámetro P_{con}. La desviación estándar $\sigma[\Delta t]$ aumenta al aumentar δ_w y disminuye al aumentar V.

6. Conclusiones

En este proyecto se ha aplicado exitosamente el método de transformación de variables al estudio de detección de conflictos entre aeronaves en presencia de vientos inciertos. Los resultados obtenidos se han validado utilizado el método de Monte Carlo, mostrando ambos métodos resultados prácticamente idénticos.

Se han estudiado indicadores como la distancia mínima entre aeronaves, tiempo hasta la distancia mínima y duración de pérdida de separación. En particular, el parámetro de probabilidad de existencia de un conclicto ha sido de gran interés.

Aunque en el presente proyecto se ha considerado una distribución de vientos continua y uniforme, cualquier otra distribución podría ser aplicable a esta metodología.

Algunos de los resultados más relevantes obtenidos en este estudio son:

- El valor esperado de los indicadores es diferente al obtenido al aplicar un estudio determinista utilizando el viento medio. Esto se debe a la relación no líneal entre los indicadores escogidos y el viento.
- Valores altos de la velocidad aerodinámica de las aeronaves contribuye a disminuir el efecto de la incertidumbre introducida por el viento.
- La certeza de que un conflicto existe o no existe decrece cuando la dispersión del viento aumenta o la velocidad de las aeronaves decrece.

Este proyecto constituye un primer paso en el desarrollo de una metodología para gestionar la incertidumbre meteorológica en el contexto de detección y resolución de conflictos entre aeronaves.

Posibles líneas de trabajo futuro incluyen:

- Aplicación de la metodología a otros indicadores.
- Utilización de otras distribuciones de vientos. En concreto, la utilización de funciones de densidad obtenidas a partir de predicciones por conjuntos sería de gran interés.
- Aplicación de la metodología a escenarios más complejos, como trayectorias formadas por varios tramos rectilíneos o consideración de más de dos aeronaves en el mismo espacio aéreo.

- Consideración de campos de viento en los que la velocidad del viento sea diferente para cada posición.

Palabras clave

Conflicto, pérdida de separación, aeronave, espacio aéreo, sistema de gestión de tráfico aéreo, ATM, SESAR, sistema de predicción por conjuntos, transformación de variables, Monte Carlo.

Referencias

[1] *IMET - Investigating the optimal approach for future trajectory prediction (TP) systems to use METeorological uncertainty information. SESAR WP-E Project 02.40*, http://sesarinnovationdays.eu/files/2013/Posters/SID%202013%20poster%20IMET.pdf, 2013, Poster in 3rd SESAR Innovation Days (SID2013).

[2] C Bayer, H Hoel, E Von Schwerin, and R Tempone, *On NonAsymptotic Optimal Stopping Criteria in Monte Carlo Simulations*, SIAM Journal on Scientific Computing **36** (2014), no. 2, A869–A885.

[3] J Cheung, JL Brenguier, A Hally, J Heijstek, and A Marsman, *Recommendations on Trajectory Selection in Flight Planning based on Weather Uncertainty*, 5th SESAR Innovation Days, Bologna, Italy (2015).

[4] E Gutiérrez Moya and M Gutiérrez Fernández, *Estadística en la ingeniería. Probabilidad*, Digital @tres, Sevilla, 2004.

[5] RV Hogg and Craig AT, *Introduction to Mathematical Statistics*, Prentice-Hall International, Englewood Cliffs, NJ, 1995.

[6] B Lapeyre, *Introduction to Monte-Carlo Methods*, Lecture, Halmstad, Sweden (2007), 2–4.

[7] ComplexWorld Research Network, *Complexity concepts in ATM*, http://complexworld.eu/wiki/Complexity_concepts_in_ATM, 2016, from ComplexWorld Network's wiki.

[8] ———, *Uncertainty in ATM*, http://complexworld.eu/wiki/Uncertainty_in_ATM, 2016, from ComplexWorld Network's wiki.

[9] T Perlinger, *Probability Theory: Multivariate random variables*, University Lecture, Uppsala University, 2012.

[10] WH Press, SA Teukolsky, WT Vetterling, and BP Flannery, *Numerical Recipes in Fortran 77. The Art of Scientific Computing*, Fortran Numerical Recipes, vol. 1, Press Syndicate of the University of Cambridge, New York, 2 ed., 1997, pp. 180–184.

[11] JM Sloughter, T Gneiting, and AE Raftery, *Probabilistic Wind Speed Forecasting using Ensembles and Bayesian Model Averaging*, Journal of the American Statistical Association **105** (2010), no. 489, 25–35.

[12] M Steiner, *Translation of Ensemble-based Weather Forecasts into Frobabilistic Air Traffic Capacity Impact*, 2009 IEEE/AIAA 28th Digital Avionics Systems Conference, IEEE, 2009, pp. 2–D.

[13] R Vázquez and D Rivas, *Analysis of the Effect of Uncertain Average Winds on Cruise Fuel Load*, 5th SESAR Innovation Days, Bologna, Italy (2015).

[14] AL Visintini, W Glover, J Lygeros, and J Maciejowski, *Monte Carlo Optimization for Conflict Resolution in Air Traffic Control*, IEEE Transactions on Intelligent Transportation Systems **7** (2006), no. 4, 470–482.

[15] EW Weisstein, *Monte Carlo Method*, `http://mathworld.wolfram.com/MonteCarloMethod.html`, From *MathWorld.com*, a Wolfram Web Resource.

[16] JW Wittwer, *Monte Carlo Simulation Basics*, `http://www.vertex42.com/ExcelArticles/mc/MonteCarloSimulation.html`, June 2004, From Vertex42.com.